JOURNAL OF PETROLOGY | VOLUME 40 | NUMBER 9 | PAGES 1443–1462 | 1999

Simple Models of CO_2 Release from Metacarbonates with Implications for Interpretation of Directions and Magnitudes of Fluid Flow in the Deep Crust

JAY J. AGUE* AND DANNY M. RYE

DEPARTMENT OF GEOLOGY AND GEOPHYSICS, YALE UNIVERSITY, P.O. BOX 208109, NEW HAVEN, CT 06520-8109, USA

RECEIVED OCTOBER 1, 1998; REVISED TYPESCRIPT ACCEPTED APRIL 28, 1999

Simple one-dimensional models of coupled advection–hydrodynamic dispersion–reaction are used to investigate processes of CO_2 release from metacarbonate beds during deep crustal (~8 kbar) Acadian prograde metamorphism in New England, USA. Two broad models in which reaction progress is controlled by gradients in H_2O–CO_2 fluid composition between different rock types are presented. In the first, diffusional exchange of volatiles across lithologic contacts is significant. CO_2 generated during prograde temperature (T) rise is transported away from metacarbonate layers to surrounding (1) metapelitic layers which generate H_2O by dehydration and/or (2) flow conduits (e.g. permeable layers or fractures) for externally derived, elevated X_{H_2O}/X_{CO_2} fluids. H_2O is transported from the surroundings into the metacarbonate layers and drives further mineral reaction. In the second model, reaction in metacarbonate layers is driven mostly by layer-parallel flow of external fluids with elevated X_{H_2O}/X_{CO_2} derived from, for example, dehydrating schists or outgassing magmas. For both models, the X_{CO_2} of the fluid within metacarbonate layers is generally predicted to increase with increasing grade from the Ankerite–Oligoclase to the Amphibole zones, and then decrease in the Diopside zone—key relationships that are commonly observed in the field. The slow reaction progress in metacarbonates driven by progressive dehydration of surrounding metapelite from greenschist to amphibolite facies probably requires time scales of fluid–rock interaction comparable to the duration of the Acadian orogeny (~10^6–10^7 my). Intense episodes of fluid flow through conduits such as fractures may produce veins and alteration selvages over fluid–rock interaction times as short as 10^3–10^4 years. Model results emphasize that the accuracy of field-based fluid flux estimates depends critically on correct identification of mass transport processes. The modeling suggests that reactive transport of volatiles between metacarbonate layers and their lithologically heterogeneous surroundings can account for basic T–fluid composition–reaction progress relationships observed in much of the Acadian orogen of New England. The results provide an alternative to up-T flow scenarios that account for these relationships by large, pervasive, horizontal fluid fluxes up regional T gradients.

KEY WORDS: *metamorphism; fluid flow; flow direction; carbon dioxide; numerical modeling*

INTRODUCTION

Metamorphic fluid flow in the deep crust has a profound impact on the spatial and temporal evolution of crustal rheology (e.g. Walder & Nur, 1984; Connolly, 1997; Wong *et al.*, 1997; Ague *et al.*, 1998; Balashov & Yardley, 1998); the transport of heat and non-volatile elements (e.g. Tracy *et al.*, 1983; Chamberlain & Rumble, 1988; Ferry & Dipple, 1991; Ague, 1994*a*, 1994*b*, 1995, 1997; Ague & van Haren, 1996); and the delivery of volatiles such as CO_2 to the atmosphere and shallow hydrosphere (e.g. Kerrick & Caldeira, 1998; Selverstone & Gutzler, 1993) where they may act to influence geochemical cycles and global climate. Proper interpretation of crustal orogenesis, therefore, requires a quantitative understanding of the processes, amounts, directions, and timing of mass transfer.

*Corresponding author. Telephone: +1-203-432-3171. Fax: +1-203-432-3134. e-mail: jay.ague@yale.edu

Landmark studies of reaction progress (Hewitt, 1973; Ferry, 1983; Tracy *et al.*, 1983; Baumgartner & Ferry, 1991; Ferry, 1992, 1994; Léger & Ferry, 1993) show that prograde mineral reactions in carbonate-bearing metasediments interlayered with carbonate-poor rocks were driven by infiltration of H_2O-rich fluids during Acadian orogenesis in New England (~350–400 Ma; Spear & Harrison, 1989; Lanzirotti & Hanson, 1996). Two fundamentally different regimes of fluid–rock interaction have been proposed based on the type of gradient in fluid composition responsible for reaction. (I) Gradients in fluid composition arising from fluid flow up regional temperature (T) gradients under local fluid–rock chemical equilibrium (Baumgartner & Ferry, 1991); fluid fluxes are large, pervasive, near horizontal, and confined to individual layers. (II) Gradients in fluid composition between chemically distinct rock types; mass transfer may occur by diffusion, dispersion, advection, or combinations of these processes (Hewitt, 1973).

A dominant role for Regime (I) has been inferred for much of northern New England (Baumgartner & Ferry, 1991; Ferry, 1992, 1994), although the mechanism that could maintain near-horizontal up-T flow at regional scales in the deep crust remains unknown (Hanson, 1997). Considerably less attention, however, has been focused on Regime (II). Therefore, we use simple, one-dimensional (1-D) numerical experiments to investigate basic relationships between reaction progress and directions and amounts of mass transfer in two broad Regime (II) models that allow fluid communication between intercalated rock types having different pore fluid X_{H_2O}/X_{CO_2}. A primary aim is to highlight the field-based observations of reaction progress and the laboratory-based reaction kinetics experiments needed to determine the relative roles of reaction-transport Regimes (I) and (II). The models are based on field studies of metacarbonate-bearing units in New England, including the Wepawaug Schist of south–central Connecticut (Hewitt, 1973; Tracy *et al.*, 1983; Palin, 1992; Ague & van Haren, 1996), and the Waits River and Gile Mountain Formations of central–eastern Vermont (Ferry, 1992, 1994).

The basis of the first model is that metamorphic X_{H_2O}/X_{CO_2} at metacarbonate–schist and metacarbonate–quartz vein contacts was commonly higher than that in metacarbonate interiors throughout much of the upper greenschist to amphibolite facies portion of the Wepawaug Schist (Hewitt, 1973; Vidale & Hewitt, 1973; Tracy *et al.*, 1983). In this model, diffusional exchange of volatiles between metacarbonate layers and adjacent sources and/or conduits for elevated X_{H_2O}/X_{CO_2} fluids is significant (Fig. 1a). The advective component of transport is not required to be up-T, layer-parallel, or horizontal. CO_2 generated during prograde heating is transported away from metacarbonate layers to surrounding (1) metapelitic layers, which generate H_2O by thermally driven dehydration, and/or (2) flow conduits (e.g. permeable layers or fractures) for externally derived, elevated X_{H_2O}/X_{CO_2} fluids. H_2O is transported from the surroundings into the metacarbonate layers and drives further mineral reaction. Water sources or conduits could also cross-cut or lie within metacarbonate layers.

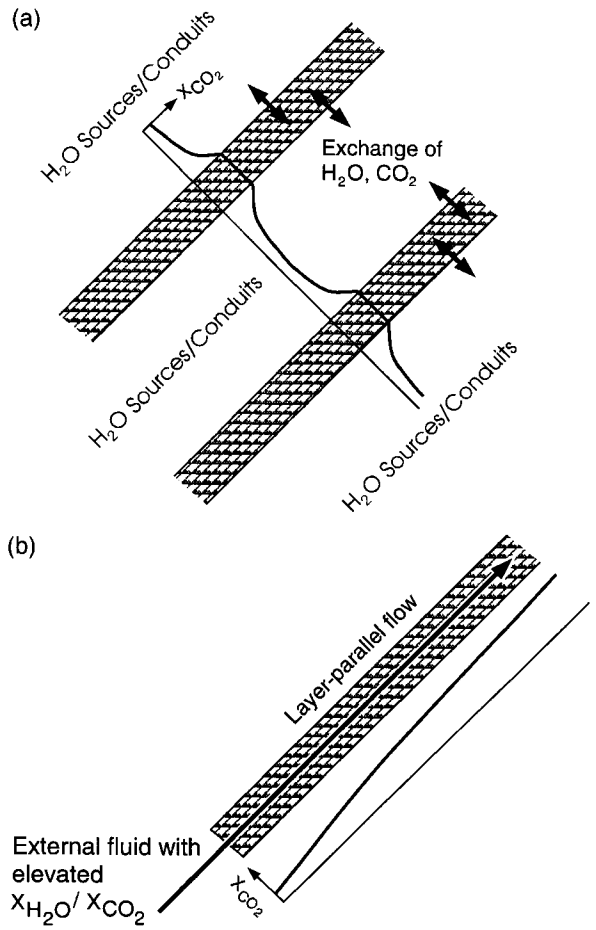

Fig. 1. Conceptual models of mass transfer. Metacarbonate layer denoted by brick pattern. Layer orientation is arbitrary. (a) Model based on Hewitt (1973) and Vidale & Hewitt (1973). Significant volatile exchange occurs between layers as a result of diffusive mass transfer. Advection is not required to be up-T, layer-parallel, or horizontal. (b) Layer-parallel flow in metacarbonate layer; negligible mass transfer perpendicular to layering. Input fluid could be derived from dehydrating schists or degassing magmas and has X_{H_2O}/X_{CO_2} higher than that in equilibrium with metacarbonate mineral assemblage.

The second model is motivated by Ferry's (1994) observations of sharp discontinuities in reaction progress between adjacent layers for some outcrops in northern New England suggesting that, in some cases, diffusional exchange between layers may be limited and that layer-parallel advection channelized along schistosity or relict bedding is important. We consider flow-dominated input

of fluids that have initial X_{H_2O}/X_{CO_2} slightly higher than that in equilibrium with the metacarbonate as a means to drive reaction progress (Fig. 1b). Possible sources for elevated X_{H_2O}/X_{CO_2} fluids include underlying dehydrating schists or degassing magmas. The fluids could be input via extensional fractures in fold hinges (see Rye & Rye, 1974), and then flow along the fold limbs (many other flow scenarios are also possible).

MODEL FORMULATION

Conservation of mass for species i (CO_2 or H_2O) in a multicomponent fluid for a fully saturated, porous flow region is given by the advection–dispersion–reaction equation (see Bear, 1972; Garven & Freeze, 1984; Lasaga & Rye, 1993; Bolton *et al.*, 1996; Ague, 1998)

$$\frac{\partial(\varphi C_i)}{\partial t} = \nabla \cdot (\varphi D_i \nabla C_i) - \nabla \cdot (\varphi \boldsymbol{v} C_i) + \varphi \sum_j R_{i,j} \qquad (1)$$

in which t is time, C is concentration, $\boldsymbol{v}$ is the pore fluid velocity, D is the hydrodynamic dispersion coefficient that incorporates the effects of both molecular diffusion (including tortuosity) and dispersion, φ is porosity, and $R_{i,j}$ is the production rate (positive) or consumption rate (negative) of i as a result of chemical reaction j (Table 1). The first term on the right-hand side of the equation describes mass transport by diffusion and dispersion (hydrodynamic dispersion); the second term describes transport by fluid advection; and the third term describes fluid–rock reactions. We solve the 1-D version of equation (1) in which transport is parallel to the z-axis. Diffusion of H_2O and CO_2 through the solids is assumed negligible relative to transport in the fluid phase.

The flux of species i at any time and place is

$$\boldsymbol{Q}_i = -D_{e,i} \nabla C_i + \varphi \boldsymbol{v} C_i \qquad (2)$$

in which $\boldsymbol{Q}_i$ is the flux and $D_{e,i}$ is the effective hydrodynamic dispersion coefficient for i given by $D_{e,i} = \varphi D_i$. The first and second terms on the right of equation (2) represent fluxes as a result of hydrodynamic dispersion and advection, respectively.

Chemical fluid–rock reactions proceed at finite rates. The local equilibrium approximation is a kinetic end-member predicated on instantaneous rates of fluid–rock equilibration. We did not assume local equilibrium and used a more general kinetic model for reaction rates in metacarbonate layers (Lasaga & Rye, 1993)

$$R_{i,j} = \left(\frac{1}{\varphi}\right) k_j \nu_{i,j} \bar{A}_{l,j} s \, |\Delta G_j|^{n_j} \qquad (3)$$

in which k_j is the intrinsic reaction rate constant for reaction j, $\nu_{i,j}$ is the stoichiometric coefficient of species i in reaction j, $\bar{A}_{l,j}$ is the surface area exposed to fluid of the rate-limiting mineral l in reaction j, $|\Delta G_j|$ is the absolute value of the Gibbs free energy change of reaction j at the T and P of interest, n_j is the reaction order for reaction j, and s is, by convention, $+1$ if ΔG_j is negative and -1 otherwise. The net production or consumption rate for i is obtained by summing over the rate expressions for all reactions j [see equation (1)]. Equation (3) does not preordain major fluid–rock disequilibrium. Local equilibrium is essentially attained if the $R_{i,j}$ are rapid relative to rates of (1) mass transport at the length scale of interest and (2) T and P change. The change in moles for a solid phase θ due to reaction j follows from equation (3):

$$\frac{\partial m_{\theta,j}}{\partial t} = k_j \nu_{\theta,j} \bar{A}_{l,j} s \, |\Delta G_j|^{n_j} \qquad (4)$$

in which m_θ is the moles of θ per unit volume of rock. The value of k_j has a strong, Arrhenius-type T dependence:

$$k_j = k_j^\circ \exp\left[\frac{-Ea_j}{R}\left(\frac{1}{T} - \frac{1}{T^\circ}\right)\right] \qquad (5)$$

in which k_j° is the intrinsic reaction rate constant at some convenient reference temperature T°, Ea_j is the activation energy for reaction j, and R is the gas constant.

The fluid flow model is based on mass conservation for a fluid in a porous medium (see Walder & Nur, 1984; Bolton *et al.*, 1996; Hanson, 1997):

$$\frac{\partial(\rho_f \varphi)}{\partial t} = -\nabla \cdot (\rho_f \boldsymbol{q}) + \left(\frac{\partial M_f}{\partial t}\right)_{\text{Rxn, HDisp}} \qquad (6)$$

in which $\boldsymbol{q}$ is the volumetric flow rate per unit area, ρ_f is the fluid density, and M_f is mass of fluid per unit volume. The first term on the right of equation (6) accounts for fluid mass changes as a result of fluid flow, whereas the second accounts for mass changes caused by chemical reaction and hydrodynamic dispersion. For the fluid flow term, $\boldsymbol{q}$ is related to pore fluid pressure (P_f) by Darcy's law (z-axis vertical):

$$\boldsymbol{q} = -\frac{\kappa}{\mu}(\nabla P_f - \rho_f \boldsymbol{g}) \qquad (7)$$

in which κ is the permeability (assumed scalar), μ is the fluid viscosity, and $\boldsymbol{g}$ is the acceleration of gravity. The pore velocity $\boldsymbol{v}$ is given by $\boldsymbol{v} = \boldsymbol{q}/\varphi$. Walder & Nur (1984) showed that the rate of porosity change can be cast in terms of reversible and irreversible components:

$$\frac{\partial \varphi}{\partial t} = \varphi \beta_\varphi \left(\frac{\partial P_f}{\partial t}\right) + \left(\frac{\partial \varphi}{\partial t}\right)_{\text{Irrev}} \qquad (8)$$

in which β_φ is a 'pore compressibility' for the rock

Table 1: List of symbols

Symbol	Definition	Units*
i	Fluid species index (H_2O or CO_2)	
j	Reaction index	
k	Generalized reaction rate constant for Da_{II}	t^{-1}
k_j°	Intrinsic rate constant for j	mol L^{-2} t^{-1}[E mol^{-1}]$^{-n_j}$
k_j°	Intrinsic rate constant for j at T°	mol L^{-2} t^{-1}[E mol^{-1}]$^{-n_j}$
m_θ	Moles of θ per unit volume rock	mol L^{-3}
n_i	Moles of i produced or consumed	mol L^{-3}
n_j	Reaction order for j	
q_{TI}	Time-integrated fluid flux	L^3 L^{-2}
s	Kinetic sign convention	
$\bar{A}_r$	Rate-limiting surface area	L^2 L^{-3}
C	Concentration	mol L^{-3}
D	Hydrodynamic dispersion coefficient	L^2 t^{-1}
D_e	Effective hydrodynamic dispersion coefficient	L^2 t^{-1}
D_f	Diffusion coefficient	L^2 t^{-1}
Da_{II}	Dämkohler-II number	
Ea	Activation energy	E mol^{-1}
ΔX_{CO_2}	difference in X_{CO_2} between downstream contact and inlet	
ΔG	Free energy change of reaction	E mol^{-1}
M_f	Mass fluid per unit volume rock	M L^{-3}
P_f	Fluid pressure	P
R	Gas constant	E mol^{-1} K^{-1}
$R_{i,j}$	Reaction rate for species i, reaction j	mol L^{-3} t^{-1}
$R_{H_2O,Dehy}$	Dehydration rate	mol L^{-3} t^{-1}
T°	Kinetic reference temperature	K
ΔT	Temperature interval for devolatilization	K
$\bar{V}_f$	Molar volume of fluid	L^3 mol^{-1}
X_i	Mole fraction i in fluid	
α_L	Longitudinal dispersivity	L
β_ϕ	Pore compressibility	P^{-1}
δ	Characteristic length scale	L
θ	Index for solid phase	
κ	Permeability	L^2
κ_0	Initial permeability	L^2
μ	Viscosity	P t
ν	Stoichiometric coefficient	
ρ_f	Fluid density	M L^{-3}
ρ_{rk}	Bulk-rock density	M L^{-3}
τ	Tortuosity coefficient for φ	
φ	Porosity	
φ_0	Initial porosity	
χ_w	Total H_2O release during metapelite dehydration	M H_2O (M Rock)$^{-1}$
$\boldsymbol{q}$	Fluid flux vector	L^3 L^{-2} t^{-1}
$\boldsymbol{v}$	Pore velocity vector	L t^{-1}
v_z	z component of pore velocity	L t^{-1}
$\boldsymbol{g}$	Acceleration of gravity	L t^{-2}
$\boldsymbol{Q}_i$	Flux vector for species i	mol L^{-2} t^{-1}

*Abbreviations: E, energy; mol, moles; M, mass; L, length; P, pressure; t, time; K, Kelvin.

matrix. The first term on the right accounts for reversible expansion or collapse of pore space related to changes in P_f. The second term represents irreversible changes caused by, for example, crystalline plasticity, pressure solution, non-volatile element metasomatism, and volume changes during reaction (see Walder & Nur, 1984; Wong *et al.*, 1997). Substantial progress has been made in modeling irreversible φ changes (e.g. Walder & Nur, 1984; Connolly, 1997; Wong *et al.*, 1997; Balashov & Yardley, 1998), but major uncertainties remain, particularly those surrounding pressure solution and larger-scale forms of non-volatile element mass transfer. Consequently, we have neglected irreversible φ changes. Feedbacks between κ and reversible changes in φ were modeled using $\kappa = \kappa_0(\varphi/\varphi_0)^3$ (Wong *et al.*, 1997). Here, κ_0 and φ_0 are the initial perrmeability and porosity, respectively, and the exponent 3 is thought to be appropriate for opening and closing of microcracks in low-porosity rocks (David *et al.*, 1994).

Numerical solution of the governing equations is summarized in Appendix A.

CHEMICAL REACTIONS

The sedimentary precursors to the metacarbonate layers we modeled were probably 'impure' limestones or marls composed mostly of calcite, dolomite, quartz, albitic plagioclase, and clay minerals, with minor amounts of oxide minerals, sulfide minerals, and organic matter. Ferry (1992) showed that five reactions dominated the prograde metamorphism of this protolith, and that these reactions are excellent models for the regional Ankerite–Oligoclase, Biotite, Amphibole, and Diopside zones in the Waits River Formation of Vermont, USA. A similar zonal sequence is recognized widely elsewhere in New England, such as in the Wepawaug Schist of Connecticut, USA (Hewitt, 1973; Tracy *et al.*, 1983; Palin, 1992). The five model reactions of Ferry (1992) are the basis for our numerical experiments; these reactions involve albite (Ab), anorthite (An), calcite (Cc), diopside (Di), dolomite (Dol), muscovite (Ms), paragonite (Pg), phlogopite (Phl), quartz (Qtz), and tremolite (Tr). They are

(1) $Pg + Cc + 2Qtz = Ab + An + CO_2 + H_2O$ (Ankerite–Oligoclase zone)

(2) $Ms + 3Dol + 2Qtz = Phl + An + 2Cc + 4CO_2$ (Biotite zone)

(3) $5Dol + 8Qtz + H_2O = Tr + 3Cc + 7CO_2$ (Amphibole zone)

(4) $Tr + 3Cc + 2Qtz = 5Di + 3CO_2 + H_2O$ (Diopside zone)

(5) $Phl + 3Cc + 6Qtz = 3Di + Kfs + 3CO_2 + H_2O$ (Diopside zone).

Because zoisite (Zo) (or clinozoisite) is present in some upper greenschist- to amphibolite-facies metacarbonate rocks (Hewitt, 1973; Ferry, 1992), we also considered

(6) $3An + Cc + H_2O = 2Zo + CO_2$.

Unless otherwise noted, the initial rock mode was based on general modal relationships observed at many localities in New England (Hewitt, 1973; Ferry, 1992, 1994): 40% Cc; 40% Qtz; 10% plagioclase (An_{10}); 7% Dol; 3% mica (2·75% Ms; 0·25% Pg).

Thermodynamic data, the modeling of H_2O–CO_2 fluids, activity models for minerals, and chemical kinetic rate parameters are discussed in Appendix A.

TEMPERATURE–TIME PATHS

We investigated several prograde temperature–time (T–t) paths compatible with physical models of regional metamorphism (e.g. Hanson, 1997). The constant T increase of 20°C/my was generally used. The heats of mineral reactions were not computed; these effects were assumed to be incorporated into the specified T–t path. T gradients along transport pathways were not considered for two reasons. First, T gradients have a small impact on fluid flow given that T values at each end of a typical model flow region of 50 m length would differ by only 0·5–1·5°C for T gradients of 10–30°C/km. Second, gradients in fluid composition as a result of T gradients tend to be overshadowed by the gradients in fluid composition between model metacarbonate layers and model schists or flow conduits. To drive reaction from the Ankerite–Oligoclase zone through the Diopside zone by purely advective, up-T flow requires time-integrated fluxes (q_{TI}) of ~10^5–10^6 cm^3/cm^2 (Ferry, 1992, 1994; Léger & Ferry, 1993). In contrast, the maximum q_{TI} for our simulations is ~5×10^4 cm^3/cm^2 (for most simulations, q_{TI} is <~200 cm^3/cm^2). Thus, neglect of T gradients in our simple models is reasonable.

METACARBONATE LAYER INTERCALATED WITH DEHYDRATING PELITIC LAYERS

This section focuses on 'conservative' flow scenarios for low-permeability rocks. A central aim is to determine if substantial reaction progress is possible when cross-layer diffusion of volatiles is important and advection through metacarbonate layers is limited (Figs 1a and 2a). To this end, we modeled a metacarbonate layer intercalated with dehydrating metapelitic rocks (Fig. 2a). The H_2O necessary for decarbonation was generated within the flow region by dehydration. The H_2O and CO_2 from internal devolatilization produced pressure gradients that

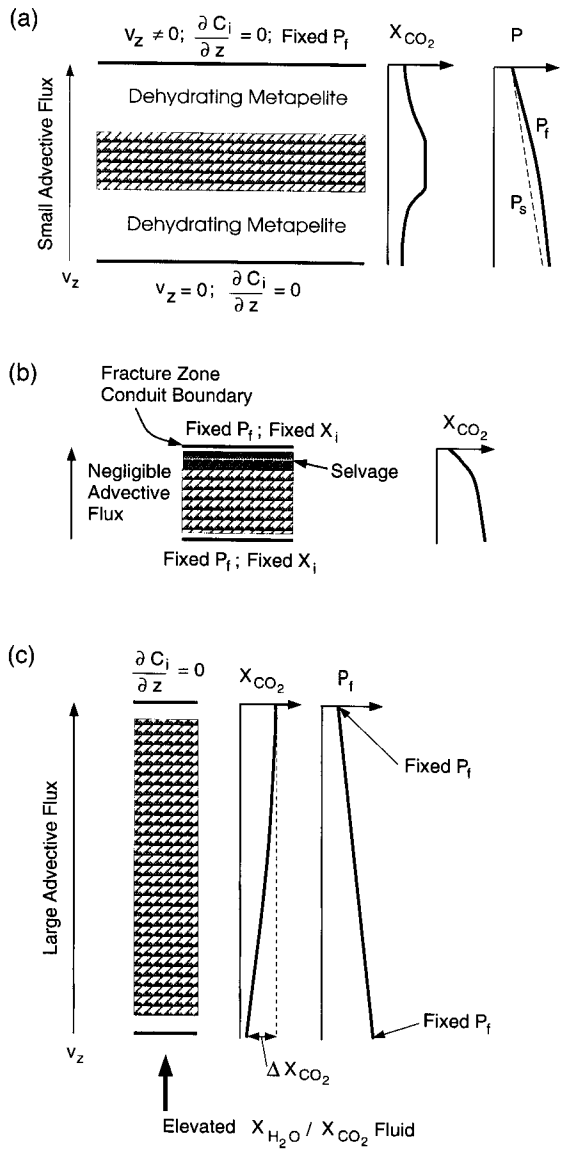

Fig. 2. Boundary conditions for devolatilizing metacarbonate layer (brick pattern) simulations. v_z, z-component of pore velocity; P_f, fluid pressure; P_s, solid pressure. (a) Metacarbonate layer surrounded by dehydrating metapelite layers. P_f is always close to P_s (within ~10 bars), but P_f gradients diverge from lithostatic gradient. P_f gradients driving flow result from devolatilization of metacarbonate and metapelite layers within the flow region. Generalized fluid composition profile also shown. (b) Model set-up for Wep-8g simulation. (c) Layer-parallel flow in metacarbonate layer; input fluid has X_{H_2O}/X_{CO_2} higher than that in equilibrium with metacarbonate mineral assemblage.

drove fluid flow upward and out of the system, but no transport of external H_2O or CO_2 into the system occurred. Because of the importance of diffusion, the results are largely independent of the orientation of the layers and the advection direction.

Natural systems consist of many intercalated metacarbonate and metapelite layers. However, modeling of such systems is computationally expensive. Our models involve a single metacarbonate layer, but were set up so that fluid composition gradients around the layer would be similar to those expected for systems of multiple metacarbonate–metapelite interbeds in which cross-layer advective fluxes are small and cross-layer diffusion is important (see Figs 1a and 2a). Thus, we obtain results relevant for multiple metacarbonate–metapelite interbeds by modeling only one metacarbonate layer.

Initial and boundary conditions

Following Hanson (1997), dehydration was assumed to proceed linearly over a specified T interval ΔT such that the third term on the right of equation (1) becomes

$$\varphi \sum_j R_{i,j} = \varphi R_{H_2O,Dehy} = \frac{\chi_w \rho_{rk}}{18 \Delta T} \frac{dT}{dt} \quad (9)$$

in which $R_{H_2O,Dehy}$ is the H_2O production rate for metapelitic rock, χ_w is total H_2O release during metamorphism; ρ_{rk} is the rock density (2·85 g/cm^3; Ague, 1994*a*), and 18 is the molecular weight of water (g/mol). Metapelitic rocks of the Wepawaug Schist lost ~2 wt % volatiles, on average, in Barrovian Chlorite–Biotite zone to Kyanite zone metamorphism [data of Ague (1994*a*)]. This fluid was probably mostly H_2O because (1) carbonate minerals are rare or absent in Wepawaug metapelitic rocks (average CaO in the Chlorite and Biotite zones is 0·36 wt %; Ague, 1994*a*), and (2) most or all carbonate is reacted out of the metapelites by the time the lowest-grade metacarbonate reaction [reaction (1)] begins in the Barrovian Garnet zone. Point (2) may also be relevant for some northern New England localities (see Ferry, 1994). Léger & Ferry (1993) estimated that metapelites of the Waits River Formation lost 3 wt % H_2O during Ankerite–Oligoclase zone to Amphibole zone metamorphism of intercalated metacarbonate rocks. Unless noted otherwise, we used an intermediate χ_w value of 2·5 wt % (0·025 g H_2O/g rock) based on the Ague (1994*a*) and Léger & Ferry (1993) results. Because dehydrating metapelites may produce some CO_2, we also study generation of representative H_2O–CO_2 fluids in model metapelites. Dehydration rates at lithologic contacts are a function of many variables, including the compositions of fluids and mineral solid solutions (see Walther, 1996). Our simplified treatment is probably adequate, however, because we are focused on basic aspects of reaction progress in lithologically heterogeneous settings.

The model boundaries were placed at fixed distances from the center of the metacarbonate layer and had $\partial C_i/\partial z = 0$ for $t \geq 0$. Thus, no hydrodynamic dispersion of CO_2 or H_2O occurred across the boundaries (Fig. 2a). P_f was fixed at the initial value for the downstream

boundary for $t \geq 0$. A no-flow boundary condition was used at the upstream contact ($\nabla P_f = \rho_f \boldsymbol{g}$) for $t > 0$, yielding $v_z = 0$ there. Consequently, advection could occur across the downstream boundary, but not the upstream boundary (Fig. 2a).

The initial P_f at the center of the metacarbonate layer was 7·8 kbar based on thermobarometry results for the Waits River Formation (Ferry, 1994). This P_f is also appropriate for the Wepawaug Schist (7–9 kbar; Ague, 1994*b*). Initial permeability (κ_0) was varied between the small but geologically reasonable values of 1×10^{-18} and 2×10^{-18} cm^2 (see Connolly, 1997) such that pore velocities were small and P_f values were always close to rock pressure (within ~10 bars). The initial P_f gradient was set to the lithostatic pressure gradient. Other initial gradients (e.g. hydrostatic) have no impact on the results because model P_f gradients evolved rapidly away from the initial conditions ($t \sim 10^2$ years) and diverged significantly from lithostatic (Fig. 2a). Because of the no-flow boundary condition at the base of the system, the P_f generated by devolatilization drove advection vertically upward and out across the downstream boundary (Fig. 2a). This fluid had X_{H_2O}/X_{CO_2} higher than that within the metacarbonate layer, and would have contributed to devolatilization in metacarbonate layers further downstream (not modeled).

Initial T was 495°C (768·15 K) based on field observations of the onset of reaction, which is typically found in mid-greenschist facies rocks (500 ± 25°C; Ferry, 1992, 1994). The initial fluid was in equilibrium with Pg + Ms + Cc + Dol + Qtz + Pl at 495°C and 7·8 kbar. The equilibrium assumption holds if little or no change in mineral assemblage occurred between the end of diagenesis and the onset of reaction (1). ΔT was set to either 80 or 100 K based on peak T values for the Waits River Formation (~575°C; Ferry, 1992, 1994) and the Wepawaug Schist (~600°C; Ague, 1994*b*; van Haren *et al.*, 1996). Unless otherwise noted, 100 K was used.

The hydrodynamic dispersion coefficient for 1-D transport can be expressed as $D_i = D_{f,i}\tau + \alpha_L|v_z|$ (see Bear, 1972; Garven & Freeze, 1984). Here, $D_{f,i}$ is the diffusion coefficient for i in the fluid phase, τ is the tortuosity factor, α_L is the longitudinal dispersivity, and v_z is the z component of pore velocity. α_L varies widely between zero and 10^3 cm in low-permeability rocks such as shales (see Anderson, 1979). Because the model pore velocities were small, we assumed that the D_i were dominated by molecular diffusion. τ varies between ~0·1 and 1·0 (Dullien, 1979), but its value in metamorphic systems is poorly known. We set $D_i = 316$ cm^2/yr, which can be considered to be the product of a typical $D_{f,i} = 3160$ cm^2/yr (1×10^{-4} cm^2/s; see Nigrini, 1970) and $\tau = 0{\cdot}1$. This τ represents highly tortuous transport pathways; a larger τ would increase diffusional mass transfer [equation (2)]. Results for different D_i values are compared later in the paper. The pore compressibility (β_ϕ) was set to 5×10^{-4} bar^{-1} (Wong *et al.*, 1997). A representative viscosity $\mu = 5 \times 10^{-4}$ Pa s ($1{\cdot}584 \times 10^{-16}$ bar yr) was used. Initial porosity was typically 0·001; variable φ_0 (0·002–0·0005) was also considered.

Widely spaced metacarbonate layers in schist

Widely spaced metacarbonate layers that make up ~10% or less of the rock mass are common in New England (e.g. the Wepawaug Schist; Fritts, 1965). Metacarbonate layers in the Wepawaug Schist and northern New England are generally between a few centimeters and 10 m thick; we begin by considering an intermediate thickness of 5 m. This layer occupies the center of the model and is bounded on each side by 22·5 m of dehydrating metapelite. Thus, the total model length is 50 m and the volumetric metacarbonate/metapelite ratio is 0·11. κ_0 was set to 2×10^{-18} cm^2.

Fluid composition in the metacarbonate interior is close to being internally buffered (near local equilibrium) while devolatilization reactions are occurring during heating at at 20°C/my (Fig. 3). When a reactant is completely consumed, CO_2 is no longer produced and X_{CO_2} drops because CO_2 continues to be transported out of the layer while H_2O enters it. As X_{CO_2} decreases, other reactions are encountered and the central part of the layer once again approaches the internally buffered condition. This general pattern of T–X_{CO_2} evolution follows the conceptual model of Hewitt (1973). The topology of the T–X_{CO_2} diagram dictates that (1) over most of the reaction history, the curves for reactions (1)–(3) are very closely spaced, and (2) at a given T, diopside-producing reactions (4) and (5) occur at much lower X_{CO_2} than the other reactions. Consequently, the model predicts that peak X_{CO_2} should increase from the Ankerite–Oligoclase to the Amphibole zones, but then drop in the Diopside zone (Fig. 3). At T >~590°C, after reactions (4) and (5) have gone to completion, X_{CO_2} drops significantly (Fig. 3) and some Zo is produced by reaction (6). The highest T systematics of Fig. 3 are not directly applicable to northern New England (Waits River, Gile Mountain Formations) because peak T there was ~575°C (Ferry, 1994). Reactions (4) and (5) are not completed at this T, consistent with field relations in northern New England (Ferry, 1992).

Reaction progress varies systematically from the interior to the edge of the model metacarbonate layer (Fig. 4). In the Ankerite–Oligoclase and Biotite zones, reaction progress is relatively uniform across the layer but is slightly greater at its edges (Fig. 4). In the Amphibole and Diopside zones, reaction progress is significantly greater at the layer edges than in the interior, leading to metasomatic zoning. For example, at $t = 2{\cdot}6$ my, the

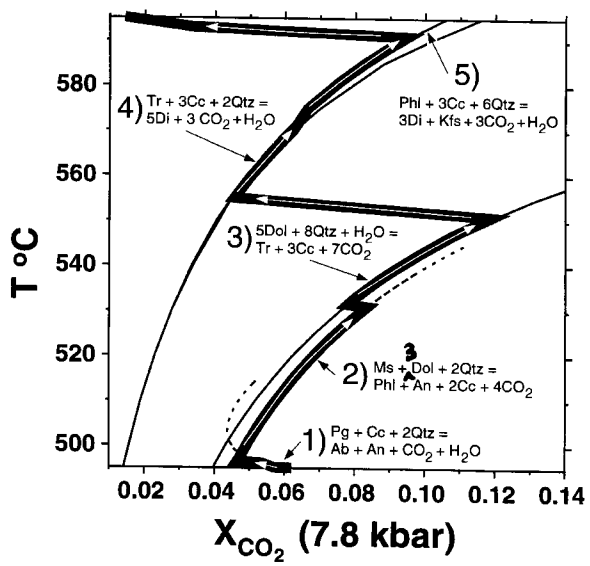

Fig. 3. Evolution of fluid composition during prograde T increase (bold continuous line) for interior of metacarbonate layer of 5 m thickness. Reactions (1)–(5) from the text are labeled. Curves for reactions (1) and (2) are dashed because their positions depend upon plagioclase composition. T–X_{CO_2} path during heating denoted by white arrows. Ab, albite; An, anorthite; Cc, calcite; Di, diopside; Dol, dolomite; Kfs, K-feldspar; Ms, muscovite; Pg, paragonite; Phl, phlogopite; Qtz, quartz; Tr, tremolite.

amphibole-producing reaction (3) has ceased in the outer portions of the layer (all Dol has been consumed), whereas the interior retains most of its Dol and little amphibole has been produced (Fig. 4). Buffering capacity is lost first at the edges of the metacarbonate layer because fluid compositional gradients between the layer and its surroundings are steepest at lithologic contacts (Figs 1a and 5). Thus, X_{CO_2} at the edges will be smaller than that in the interior. This discrepancy will tend to increase over the course of a given reaction as the thicknesses of the highly reacted edge zones increase (Fig. 6). Eventually, the layer loses its buffer capacity and X_{CO_2} drops until the next reaction is intersected (see Fig. 3). The general pattern of X_{CO_2} increase from the Ankerite–Oligoclase to the Amphibole zones followed by a marked decrease in the Diopside zone holds for the edges and interior of the metacarbonate layer (Fig. 6).

Advection of fluid into the metacarbonate layer at the upstream contact (−2·5 m in Fig. 4) slightly advances reaction progress there relative to the downstream contact. The effect is small because model pore velocities are relatively small; average v_z across the model lithologic contacts is ~0·04 cm/yr. A Peclet number ($= v_z\delta/D_i$) calculated using v_z = 0·04 cm/yr, D_i = 316 cm^2/yr, and a characteristic length scale δ = 25 m = 2500 cm (the half-width of the flow region) is ~0·3. This value illustrates the important role of cross-layer diffusion: the models predict diffusion and reaction over considerable distances on 10^6–10^7 year time scales (Fig. 4). Field studies of oxygen isotope fronts (e.g. Bickle *et al.*, 1997, p. 1502) indicate that such length scales are realistic.

Reaction fronts

At low grades, reaction fronts are broad and mineral abundances and assemblages are fairly uniform across the layer, but at higher grades, fronts are sharper and significant spatial zonation of assemblages is predicted (Fig. 4). Two main factors control the spatial distribution of assemblages. (1) Solid solution in plagioclase is important for the two low-grade reactions [reactions (1) and (2); see Appendix A]. Solid solution tends to broaden reaction fronts and reduce spatial zonation of mineral assemblages. (2) The interplay between reaction rates and transport plays a key role in determining the shape of reaction fronts and is often summarized by Dämkohler numbers (Boucher & Alves, 1959). The Dämkohler-II number, for example, compares rates of reaction and diffusion

$$\mathrm{Da_{II}} = \frac{\delta^2 k}{D_i} \qquad (10)$$

in which k is a reaction rate constant and δ a characteristic length scale. Large $\mathrm{Da_{II}}$ implies that reaction rates are 'fast' relative to mass transport rates and that the fluid–rock system is close to local equilibrium. A small $\mathrm{Da_{II}}$ implies the opposite. For example, increasing the reaction rate and/or decreasing D_i will increase $\mathrm{Da_{II}}$, decrease the length scale over which fluid and rock are out of equilibrium, and therefore sharpen reaction fronts. In addition to the lack of solid solution effects, the sharpening of fronts for the higher-T reactions (3)–(5) is also a consequence of two kinetic factors that increase rates with grade. First, reaction rates increase with T because of the strong T dependence of the Arrhenius term in the kinetic rate expression [equation (5)]. Second, the lower-T reactions generally proceed under fairly water-rich conditions (X_{CO_2} < 0·085). Thus, fluid compositional gradients between the metacarbonate layer and its surroundings are small, decreasing the ΔG term in the rate expression and overall reaction rates.

Fronts for reactions (3)–(5) would propagate as 'step' functions under perfect local fluid–rock equilibrium (infinite Dämkohler numbers). The boundaries between completely reacted and unreacted zones would be knife-sharp (see Ague, 1998). The T–X_{CO_2} evolution of the model metacarbonate layer (see Fig. 3) would, however, remain nearly unchanged. Dämkohler numbers would increase if larger reaction rate constants, larger rate-limiting surface areas, and/or smaller porosities were used relative to default model values [equation (3) and Appendix A]. Furthermore, fronts would tend to sharpen if the reaction kinetics were linear [n_j = 1 in equation

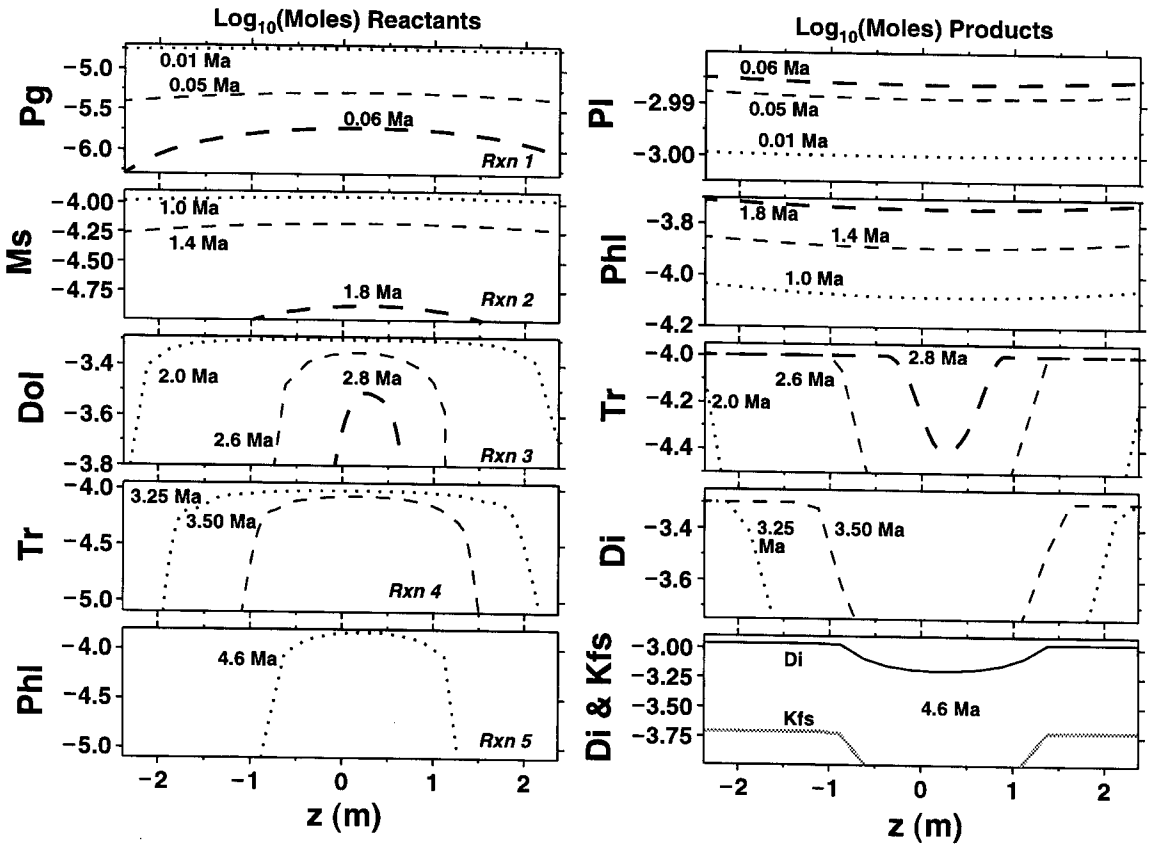

Fig. 4. Amounts of key reactants (left panels) and products (right panels) for reactions (1)–(5) at various model times for metacarbonate layer of 5 m thickness. Upstream contact between metacarbonate layer and metapelite is at left; downstream contact is at right. It should be noted that reaction fronts are more pronounced for reactions (3)–(5) than for reactions (1) and (2). Pg, paragonite; Pl, plagioclase; Ms, muscovite; Phl, phlogopite; Dol, dolomite; Tr, tremolite; Di, diopside; Kfs, K-feldspar.

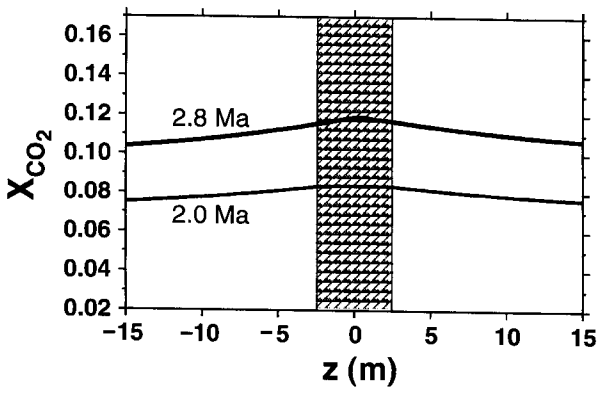

Fig. 5. X_{CO_2} profiles for reaction (3) at model times of 2·0 and 2·8 my. Position of metacarbonate layer denoted by brick pattern.

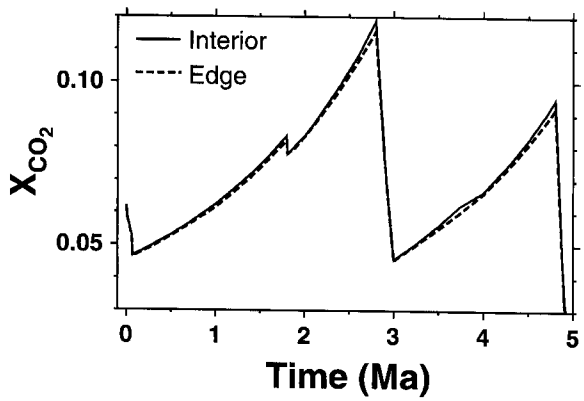

Fig. 6. X_{CO_2} vs model time for metacarbonate layer of 5 m thickness. Continuous line, maximum X_{CO_2} in metacarbonate interior; dashed line, X_{CO_2} for metacarbonate edge at upstream contact with model metapelite.

(3); Lasaga & Rye, 1993; Ague, 1998). If local equilibrium is effectively attained for reactions involving minor solid solution effects, then reaction fronts will be sharp and may be misinterpreted to be primary lithologic contacts in the field (see Ague, 1998).

Temperature–time path

The effect of different T–t paths on reaction progress was investigated using several constant rates of T increase

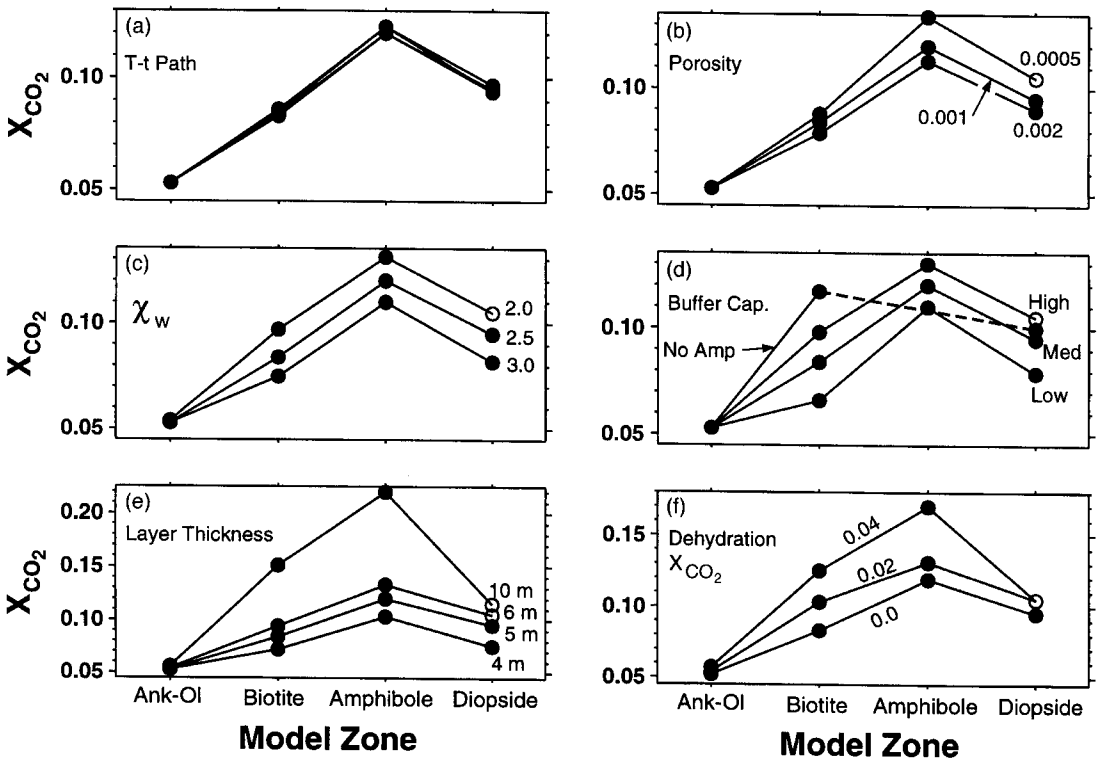

Fig. 7. Peak X_{CO_2} reached in interior of metacarbonate layer for model Ankerite–Oligoclase (Ank–Ol), Biotite, Amphibole, and Diopside zones. ●, reaction complete; ○, reaction incomplete at end of simulation. (a) Curves for constant T increases of 15, 20, and 25°C/my, and for case where rate of T increase diminishes with time (see text). (b) Effect of changing porosity for initial porosities of 0·0005, 0·001, and 0·002. (c) Effect of changing χ_w for χ_w values of 2·0, 2·5, and 3·0 wt %. (d) Effect of changing initial rock buffer capacity. 'Medium' (Med) buffer capacity: 2·75% Ms; 7% Dol; 40% Qtz; 40% Cc; 10% Pl (An_{10}); 0·25% Pg. 'Low' buffer capacity: 1·75 vol % Ms; 6% Dol; 42% Qtz (other phases same percentage as in Medium buffer capacity case). 'High' buffer capacity: 3·75% Ms; 8% Dol; 38% Qtz (other phases same percentage as in Medium buffer capacity case). 'No amphibole' (No Amp): 4·75% Ms; 6·51% Dol; 38·49% Qtz (other phases same percentage as in Medium buffer capacity case). (e) Effect of changing layer thickness, for model metacarbonate layers of 4, 5, 6, and 10 m thickness. (f) Effect of dehydration fluid X_{CO_2} = 0·0, 0·02, and 0·04.

(15, 20, and 25°C/my). Furthermore, because rates of T increase may tend to diminish as peak T is approached (see Hanson, 1997), we considered a representative (but none the less arbitrary) T–t path for which the rate of T increase diminishes smoothly from 25°C/my at t = 0 my to 10°C/my at t = 5 my and 5°C/my at t = 10 my. Fluid composition evolves in a very similar manner for all four cases (Fig. 7a). The time needed for reaction increases as heating rate decreases; total model times for the 15, 20, and 25°C/my cases are about 6·3, 4·8, and 3·8 my, respectively. About 6·3 my is required for the case in which the rate of T increase diminishes with time. We note in this context that the duration of Acadian metamorphism and fluid flow was probably 10^5–10^7 years (England & Thompson, 1984).

Porosity

Initial porosity was varied from 0·0005 to 0·002 (varying φ also changes $D_{e,i}$). The calculations of Connolly (1997) suggest that this is a reasonable φ range for low-permeability crustal rocks. Maximum reversible φ changes are 0·4% relative to initial porosity. Increasing the value of φ increases the mass flux of species i [equation (2)], which increases reactant consumption. Thus, buffer capacities are exhausted more rapidly and both the peak T and the peak X_{CO_2} for a given mineral reaction tend to be decreased relative to lower-φ systems (Fig. 7b). Decreasing the value of φ tends to increase reaction time, peak T, and peak X_{CO_2} for a given reaction (Fig. 7b). For φ_0 = 0·0005, rock buffer capacity is nearly exhausted after ΔT = 100 K (5 my); reaction (4) has completed, and 99·7% of the limiting reactant for reaction (5) (Phl) has been consumed. Incompletely reacted assemblages that retain amphibole and/or biotite are ubiquitous in the Diopside zone of the Waits River Formation (Ferry, 1992; Léger & Ferry, 1993) and are also found in the Diopside zone of the Wepawaug Schist (Ague & van Haren, 1996).

Dehydration rate

The effects of different dehydration rates were examined by varying χ_w from 2 to 3 wt % (Fig. 7c). For χ_w = 2·5 wt %, the cumulative amounts of dehydration are 0·033, 0·93, 1·43, and 2·40 wt % after completion of reactions (1), (2), (3), and (4) + (5), respectively. Increasing χ_w increases dehydration rate, the X_{H_2O} of the metapelite layers surrounding the metacarbonate layer, and local concentration gradients between metacarbonate and metapelite. Equation (2) indicates that increased concentration gradients will increase the mass flux of species *i*. Therefore, a given reaction will tend to go to completion sooner, and the peak T and X_{CO_2} for the reaction will decrease relative to lower-χ_w systems (Fig. 7c). For the χ_w = 2 wt % example, reaction (4) has gone to completion whereas ~75% of the limiting reactant for reaction (5) (Phl) has been consumed after ΔT = 100°C (5 my).

Buffer capacity

Increasing the amounts of Ms and Dol in the model protolith increases rock buffer capacity, the time needed for a given reaction to be completed, and the peak T and peak X_{CO_2} relative to lower buffer capacity rocks (Fig. 7d). After ΔT = 100 K (5 my) for the high buffer capacity example (Fig. 7d), reaction (4) has completed but reaction (5) has not. In nature, ankerite is sometimes consumed completely by reactions analogous to reaction (2), and no amphibole is produced at higher grades by reaction (3) (Hewitt, 1973; Ferry, 1992, p. 54). An example of this high Ms/Dol ratio case suggests that peak X_{CO_2} will increase from the Ankerite–Oligoclase to the Biotite zone, but then decrease in the Diopside zone (Fig. 7d). The effects of increasing the metacarbonate layer thickness while keeping the mode constant (Fig. 7e) resemble the effects of increasing the modal amounts of the reactants Ms and Dol while keeping layer thickness constant (Fig. 7d).

Generation of H_2O–CO_2 fluids in model metapelite

We considered generation of fluids having X_{CO_2} of 0·02 and 0·04 in the metapelite by calculating H_2O production using equation (9) (χ_w = 2·5 wt %) and then adding CO_2 so that the X_{CO_2} of the fluid produced at each time step had the desired value. Increasing the X_{CO_2} decreases concentration gradients between model metapelite and metacarbonate layers and decreases the mass flux of species *i* [equation (2)], thus decreasing rates of reactant consumption. Consequently, buffer capacities are exhausted more slowly and both the peak T and the peak X_{CO_2} for a given mineral reaction tend to be increased relative to lower-X_{CO_2} cases (Fig. 7f). Conversely, decreasing X_{CO_2} tends to decrease reaction time, peak T, and peak X_{CO_2} for a given reaction (Fig. 7f).

Thin metacarbonate–schist interbeds

In the Waits River Formation, approximately meter-scale metacarbonate and metapelitic–metapsammitic layers tend to be closely intercalated and outcrops may have high metacarbonate abundance (Ferry, 1994). We model four representative cases using regions of 5, 4, 3, and 2 m length containing a central metacarbonate layer of 1 m thickness bounded on both sides by dehydrating metapelite. The model metacarbonate/metapelite ratios are thus 0·25, 0·33, 0·50, and 1·0. The problems were set up as described in the 'Initial and boundary conditions' section, except that ΔT = 80°C and χ_w = 3·0 wt % (more appropriate for the Waits River Formation) and that $\kappa_0 = 1 \times 10^{-18}$ cm^2.

Predicted peak X_{CO_2} increases from the Ankerite–Oligoclase to the Amphibole zone and then drops in the Diopside zone for metacarbonate/metapelite ratios of 0·25 and 0·33 (Fig. 8a). For ratios of 0·5 and 1·0, dehydration fluids are exhausted (after 4 my) before diopside-producing reactions begin (Fig. 8a). Diffusion dominates the mass transfer; total q_{fl} are less than ~20 cm^3/cm^2 for the Fig. 8a examples. Increasing the metacarbonate/metapelite ratio decreases the relative amount of H_2O generated by dehydration and decreases fluid composition gradients at model lithologic contacts. Typical $|\partial X_{CO_2}/\partial z|$ values are 10^{-7}–10^{-6} cm^{-1}, as much as 10–100 times less than for the smaller metacarbonate/metapelite ratio cases discussed previously (see Fig. 5). Smaller concentration gradients yield smaller diffusional mass fluxes [equation (2)]. For the largest metacarbonate/metapelite ratio case, fluxes are so small that phlogopite is still forming when dehydration fluids are exhausted, and no tremolite or diopside is produced (Fig. 8a). We note in this regard that Cc + Dol + Qtz + Phl + Ms + Pl assemblages may persist well into the amphibolite facies in southern and northern New England (Hewitt, 1973; Palin, 1992; Ferry, 1994), and may be valuable indicators of relatively limited interaction between metacarbonates and elevated X_{H_2O}/X_{CO_2} fluids. The predicted mineralogical zonation across the 1 m thick metacarbonate layer (Fig. 8b) is less than that for the 5 m example (Fig. 4) owing mostly to the reduced layer thickness relative to characteristic transport-reaction distances and also to the small concentration gradients which reduce ΔG and reaction rates.

Some outcrops of Waits River Formation metacarbonates contain little or no metapelite, although quartz veins are ubiquitous (Ferry, 1994). For these very high metacarbonate–metapelite outcrops, dehydration of locally intercalated metapelites would have been insufficient to drive observed reaction progress. However, the reactions could have proceeded if water was supplied by dehydration of more voluminous metapelite underlying the high metacarbonate–metapelite outcrops, or by degassing of magmas. The elevated X_{H_2O}/X_{CO_2} fluids could

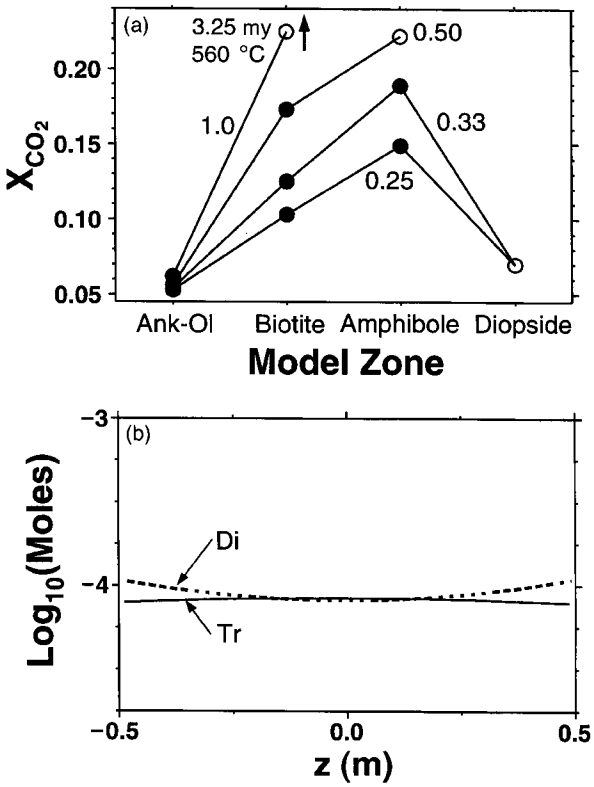

Fig. 8. Metacarbonate layer of 1 m thickness. (a) Peak X_{CO_2} for metacarbonate/metapelite ratios of 0·25, 0·33, 0·50, and 1·0. ●, reaction complete at end of simulation (model t = 4 my); ○, reaction incomplete. X_{CO_2} for metacarbonate/metapelite = 1·0 shown for t = 3·25 my; X_{CO_2} at t = 4·0 my plots off-scale. (b) Abundance of diopside (Di) and tremolite (Tr) across model metacarbonate layer for metacarbonate/metapelite ratio = 0·33 at 4·0 my. Modal variations are subtle.

have been input by diffusion in the fluid phase or, over longer length scales, by pervasive or channelized fluid flow through the metacarbonate layers or through adjacent rock units or fractures. Examples of flow-dominated transport are presented in later sections.

Conceptual 2-D transport model

Because cross-layer advective fluxes are small, the results (Figs 3–8) can be extended to the case of diffusion-dominated transport perpendicular to layers with advection-dominated transport parallel to layers. Let us consider Fig. 1a for the situation of layer-parallel advection in the metapelite layers surrounding the metacarbonate layers. CO_2 derived from metacarbonate layers will exchange (primarily by cross-layer diffusion) with H_2O generated by dehydration of the surrounding metapelite. Flow of elevated X_{H_2O}/X_{CO_2} fluids in conduits could also be important. Because CO_2 is constantly diluted by H_2O from the dehydrating surroundings in the direction of advection, a near steady-state distribution of fluid compositions develops with time. X_{CO_2} profiles perpendicular to layering at different depths will resemble each other and have the 'bell-shape' found for the 1-D cases (see Figs 1a, 2a and 5).

The conceptual model requires that changes in fluid composition as a result of T gradients along the flow path be overshadowed by local gradients in fluid composition perpendicular to layering between different rock types. At the regional scale, the layer-parallel q_{TI} in the rocks surrounding the metacarbonates could be large, although the layer-perpendicular q_{TI} need not be. The situation is more complex because the amounts and compositions of fluids generated by the metacarbonate and metapelite layers will vary spatially as different reactions operate at different crustal depths. Two-dimensional models are required to assess these and other complexities affecting regional reaction progress.

CONCENTRATION GRADIENTS ADJACENT TO FRACTURE CONDUITS

Mineralized fractures (veins) may play an important role as fluid conduits because they can: (1) support large time-integrated fluxes (~10^5–10^7 cm^3/cm^2) (Ferry & Dipple, 1991; Ague, 1994*b*); (2) have high permeability (Ague, 1995); (3) make up a significant portion of the overall rock volume (~10–30% in the amphibolite facies; Ferry, 1992; Ague, 1994*b*). Chemical and isotopic alteration of wallrocks in selvages adjacent to veins can occur if the veins are conduits for large volumes of fluid (see Meyer, 1965; Brimhall, 1977, 1979; Ague, 1994*b*, 1995, 1997; van Haren *et al.*, 1996). For example, isothermal, layer-parallel, syn-amphibolite-facies infiltration of H_2O-rich fluid along a fracture zone (now quartz veins) in a meter-scale metacarbonate bed in the Wepawaug Schist decreased $\delta^{18}O$, $\delta^{13}C$, K/Al, Na/Al, Ca/Al, Mg/Fe, and volume in diopside-rich alteration selvages of 10–15 cm width adjacent to the fracture (Tracy *et al.*, 1983; sample Wep-8g of Hewitt, 1973). We present a highly simplified model of Wep-8g selvage formation. The goal here is to examine basic reaction progress, time, and length-scale relationships applicable to natural vein selvages, not to provide a realistic model for the detailed evolution of Wep-8g.

Fluid composition, mineralogy, *T*, and *P*

We envision that X_{CO_2} in the fracture conduit was kept constant by a large, layer-parallel flux of external fluid, and that mass transfer between the metacarbonate layer and the conduit was dominated by cross-layer diffusion.

The layer-parallel flux is not explicitly modeled; we focus on the cross-layer transport (Fig. 2b). Reaction was driven by large concentration gradients between metacarbonate and fracture zone fluids (Tracy *et al.*, 1983). Large model gradients were produced by (1) setting the X_{CO_2} in the fracture zone to constant, relatively small values, and (2) setting the distance between the conduit and the metacarbonate layer to the small value of 2 cm. The advective fluxes across the boundaries are negligible and thus our results are essentially independent of layer orientation.

The little altered rock beyond the Wep-8g selvage contains mostly calcite, biotite, quartz, and plagioclase, and traces of amphibole and K-feldspar (Hewitt, 1973; Tracy *et al.*, 1983). We used a model rock layer of 1 m thickness (z = −0·5 to 0·5 m) comprising 55% Cc, 24% Phl, 12% Qtz, and 9% plagioclase (An_{40}) to represent unaltered 'protolith' (see Hewitt, 1973; Tracy *et al.*, 1983). Qtz was assumed present in excess, which is reasonable because quartz veins precipitated in the fracture conduit. We considered reactions (4)–(6) as well as an additional reaction inferred by Hewitt (1973) and Tracy *et al.* (1983):

(7) 6Cc + 5Phl + 24Qtz = 5Kfs + 3Tr + $2H_2O$ + $6CO_2$.

T was held at 590°C (863·15 K) for all model times, and the initial P_f in the center of the model layer was 8 kbar (Appendix B). The initial P_f gradient was set as described above. The initial fluid was taken to be in equilibrium with the Cc + Qtz + Phl + Pl assemblage at 590°C and X_{CO_2} = 0·11. To stay on the water-rich side of the alteration reactions, boundary conduit X_{CO_2} cannot be much above 0·07.

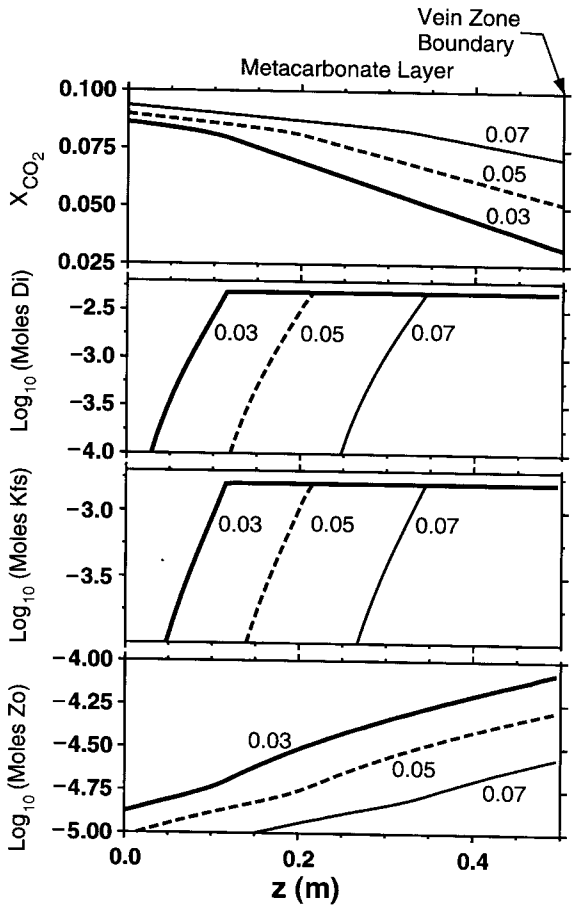

Fig. 9. X_{CO_2} and amounts of reaction products diopside (Di), K-feldspar (Kfs), and Zoisite (Zo) after 6000 model years for $\varphi_0 = 10^{-3}$; fixed X_{CO_2} = 0·11 at z = −0·502 m; P_f fixed at the initial values at both ends of the flow region; and vein zone fluid X_{CO_2} = 0·03, 0·05, and 0·07 at z = 0·502 m. Vein zone position corresponds to boundary of flow region at z = 0·502 m. Edges of model metacarbonate layer are at $z = \pm 0{\cdot}5$ m; no dehydration occurs between the boundaries and the metacarbonate edges. The selvage propagates into the metacarbonate layer from right to left. Advective fluxes in the z direction are negligible. Results for a no-flux boundary condition at z = −0·502 m ($\partial C_i/\partial z = 0$; $v_z = 0$; $t > 0$) are similar (not illustrated).

Results

The reaction products for representative simulations—Di, Kfs, and Zo—are those observed in the Wep-8g selvage (Fig. 9). Decreasing the conduit X_{CO_2} increases the difference between fluid compositions in equilibrium with the protolith assemblage and the conduit composition, thus increasing (1) $|\partial C_i/\partial z|$, (2) diffusional mass fluxes [see equation (2)], and (3) reaction progress. An important conclusion is that for reasonable ranges of conduit X_{CO_2} and rock properties, the time predicted for reaction fronts to penetrate tens of centimeters into the metacarbonate layer is only ~10^3–10^4 years.

The large concentration gradients produce large ΔG_j and large reaction rates [equation (3)]. Thus, the Di and Kfs reaction fronts are relatively sharp (Fig. 9). The Zo front is broader mostly as a result of solid solution in Pl.

The Wep-8g selvage contains minor actinolite and hornblende, but the model selvage lacks amphibole (Fig. 9). The following factors may bear on this discrepancy. First, much of the actinolite may be retrograde (Hewitt, 1973; Tracy *et al.*, 1983). Second, the hornblende is aluminous, but we do not account for Al solid solution in amphibole and, thus, our phase relations are probably oversimplified. Finally, amphibole does not form in the simulations because it is destroyed at a high rate by reaction (4). If we assume that reaction (4) does not operate (see Tracy *et al.*, 1983), then the model selvage contains Di, Tr, Kfs, and Zo (not illustrated). This example emphasizes the need for quantitative kinetic data for crustal reactions.

Our model does not account for non-volatile element metasomatism or volume loss; the intensity of these

phenomena increases progressively toward the vein contact in the Wep-8g selvage. Open system processes can play a major role in determining metamorphic evolution (see Ague, 1994*b*, 1997; van Haren *et al.*, 1996) and will be considered in future models of reaction progress.

Concentration gradients in Wep-8g were large, but smaller concentration gradients are also possible adjacent to natural veins. Results for small concentration gradients would be similar to the examples presented in previous sections; relative to Wep-8g, reaction times would increase and mineralogical zonation would be less pronounced owing to decreased diffusional mass fluxes [see equation (2)] and decreased reaction rates.

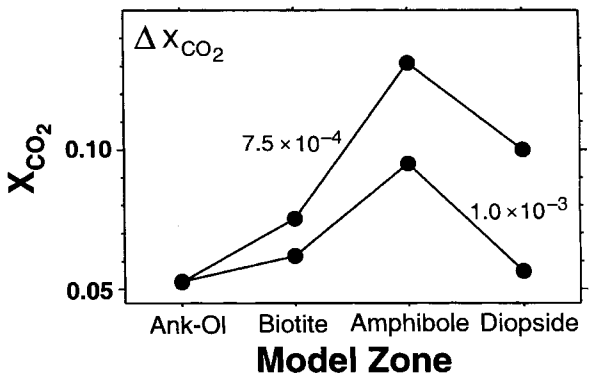

Fig. 10. Peak X_{CO_2} for models dominated by layer-parallel flow; ΔX_{CO_2} values of $1{\cdot}0 \times 10^{-3}$ and $7{\cdot}5 \times 10^{-4}$. Total model times for the $1{\cdot}0 \times 10^{-3}$ and $7{\cdot}5 \times 10^{-4}$ cases are 3·5 and 4·9 my, respectively. D_i = 316 cm^2/yr.

LAYER-PARALLEL FLOW WITHIN METACARBONATE LAYERS

We extended the 1-D model to the case of advective flow parallel to layering within metacarbonate with negligible cross-layer exchange perpendicular to the advection direction (Figs 1b and 2c). Ferry (1994) concluded that up-T flow channelized parallel to layering was important in northern New England. Our model differs from that of Ferry (1994) because reaction is driven by input of external fluids with elevated X_{H_2O}/X_{CO_2} relative to local equilibrium in metacarbonate, not by up-T flow in a T gradient within individual metacarbonate layers. The elevated X_{H_2O}/X_{CO_2} fluids could be derived from, for example, dehydrating metapelites or outgassing magmas (see Introduction).

Initial and boundary conditions

We considered an outcrop-scale, model metacarbonate layer of 10 m length. The boundaries of the flow region were fixed at a small, arbitrary distance (30 cm) from the edges of the metacarbonate (total flow region length = 10·6 m). The rock between the metacarbonate layer and the boundaries did not produce fluid. The initial P_f at the center of the flow region was 7·8 kbar and the initial P_f gradient was set as in previous sections. P_f was held constant at the boundaries for all $t \geq 0$. We set κ_0 to the relatively large value of 10^{-15} cm^2 to yield significant pore velocities (11–12 cm/yr). The simulations used an initial T of 495°C, $\varphi_0 = 0{\cdot}001$, a T increase of 20°C/my, and initial modal and chemical relations described above in 'Chemical reactions'. The P_f gradient varies little from the initial condition because of the relatively high permeability. The model pore velocities and porosities yield a Darcy flux ($v_z\varphi$) of ~10^{-2} cm^3/cm^2 per year—in the range thought typical of flow-dominated regional metamorphism (see Baumgartner & Ferry, 1991). Similar fluxes can be achieved if the P_f gradient is decreased and permeability is increased. For example, if the P_f gradient driving flow is 0·33 lithostatic and permeability is 2×10^{-15} cm^2, results are nearly identical to those presented. Fluid composition gradients were set by specifying a constant difference in X_{CO_2} (referred to as ΔX_{CO_2}) between the downstream metacarbonate contact and the inlet at the upstream boundary. We set $\partial C_i/\partial z = 0$ at the downstream boundary for all $t \geq 0$ to yield zero hydrodynamic dispersion flux there. Dispersion is important in flow-dominated systems. For exploratory purposes we compare results for D_i = 316 cm/yr ($\alpha_L = 0$) and D_i = 1500 cm/yr ($\alpha_L \sim 100$ cm).

Results

The increase in peak X_{CO_2} from the Ankerite–Oligoclase to the amphibole zones followed by a decrease in the Diopside zone is predicted for ΔX_{CO_2} values as small as $7{\cdot}5 \times 10^{-4}$ (Fig. 10). This ΔX_{CO_2} yields typical $\partial X_i/\partial z$ of ~10^{-6}/cm. Increasing ΔX_{CO_2} increases the disequilibrium between the input fluid and rock and, thus, reaction progress for a given model time (Fig. 10). Reaction fronts propagate in the direction of flow (Fig. 11). Fronts are broad for reactions (1) and (2), mainly because of solid solution in Pl (see above). Because Pl solid solution effects are dominant, increasing D_i has little effect on front shape for these reactions (not illustrated). However, increased D_i does broaden fronts for the Tr- and Di-producing reactions (Fig. 11). Total advective q_{TI} at the end of model Diopside zone reaction progress for the $\Delta X_{CO_2} = 1{\cdot}0 \times 10^{-3}$ and $\Delta X_{CO_2} = 7{\cdot}5 \times 10^{-4}$ cases (Fig. 10) are $4{\cdot}2 \times 10^4$ and $5{\cdot}6 \times 10^4$ cm^3/cm^2, respectively.

Other simulations could be performed to examine the effects of different initial and boundary conditions. None the less, the results show that gradients in input fluid composition as small as $\partial X_i/\partial z \sim 10^{-6}$/cm in layer-parallel

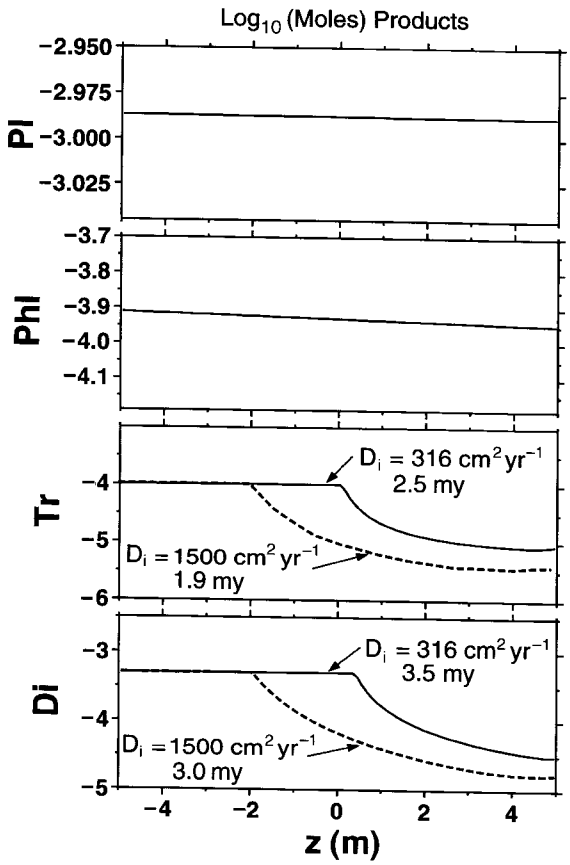

Fig. 11. Amounts of key reaction products plagioclase (Pl; at 0·03 my), phlogopite (Phl; at 1·0 my), tremolite (Tr), and diopside (Di). Results for Tr and Di shown for D_i = 316 cm^2/yr and D_i = 1500 cm^2/yr. Flow is from left to right.

flow-dominated systems are enough to drive considerable devolatilization at the scale of outcrops.

DISCUSSION

Implications for fluid fluxes and directions of flow

One advantage of numerical studies is that the reaction-transport processes, the fluid fluxes, and the spatial–temporal evolution of the models are known. Thus, model output can be used to test independently other methods of estimating fluid flow histories. For example, widely applied field-based methods that assume that reaction progress is driven by horizontal, up-T advection require positive $(\partial X_{CO_2}/\partial T)_P$ for mineral reactions and predict that X_{CO_2} and time-integrated fluid flux (q_{TI}) must increase with increasing metamorphic grade as a result of fluid production along the flow path (Baumgartner & Ferry, 1991; Ferry, 1992, 1994; Léger & Ferry, 1993). For 1-D transport and local equilibrium, the formulation is (Baumgartner & Ferry, 1991)

$$q_{TI} = \frac{\bar{V}_f[n_{CO_2} - X_{CO_2}(n_{CO_2} + n_{H_2O})]}{(\partial X_{CO_2}/\partial T)_P(dT/dx)} \quad (11)$$

in which $\bar{V}_f$ is the molar volume of the fluid and n_i is the moles of species i produced (positive algebraic sign) or consumed (negative algebraic sign) per unit volume of rock by reaction. Flow is in the positive x direction. The effects of P gradients on reaction progress are assumed to be negligible (Ferry, 1992, 1994). We used our model results as input to equation (11) to determine how well the equation estimated q_{TI}.

An important problem arose when computing $(\partial X_{CO_2}/\partial T)_P$ for reaction (1). The equilibrium boundary for the reaction is strongly dependent upon plagioclase (Pl) composition and shifts markedly as the reaction proceeds and Pl becomes richer in An. At $T \sim 500$°C [the T used to compute q_{TI} for the Ankerite–Oligoclase zone by Ferry (1992, 1994)], $(\partial X_{CO_2}/\partial T)_P$ is negative (Fig. 3). Considerable uncertainty still surrounds activity–composition relations for Pl at Ankerite–Oligoclase zone T (see Carpenter & Ferry, 1984), and our treatment of Pl is highly simplified (e.g. no compositional zoning). However, even if our prediction of negative $(\partial X_{CO_2}/\partial T)_P$ is only qualitatively correct, the advective model [equation (11)] indicates down-T flow for the Ankerite–Oligoclase zone, not up-T flow. Previous workers used constant mineral compositions to compute positive $(\partial X_{CO_2}/\partial T)_P$ and infer up-T flow in the Ankerite–Oligoclase zone (Ferry, 1992, 1994). Although we also calculate an apparent up-T q_{TI} neglecting the evolution of Pl composition, the $(\partial X_{CO_2}/\partial T)_P$ for the model Ankerite–Oligoclase zone is negative.

Apparent q_{TI} values calculated using our model output as input to equation (11) suggest up-T flow, increase with grade, and are similar to q_{TI} values calculated for the Waits River Formation in central–eastern Vermont assuming up-T flow (Fig. 12). However, no up-T flow occurs in the simulations, and the actual average model q_{TI} values are smaller than the apparent q_{TI} values (Fig. 12). Therefore, we suggest that increases in apparent q_{TI} with grade calculated using equation (11) are not a basis for distinguishing between reaction driven by fluid composition gradients between different lithologies (our simulations) and reaction driven by large, pervasive, horizontal, up-T advective fluxes confined to individual lithologic units [model of Baumgartner & Ferry (1991)]. Furthermore, q_{TI} values for a wide variety of diffusion-dominated and flow-dominated systems may be overestimated if the reaction progress is incorrectly assumed to be driven by up-T flow and interpreted using equation (11) (Fig. 12). This result emphasizes the important fact that processes of mass transport must be determined

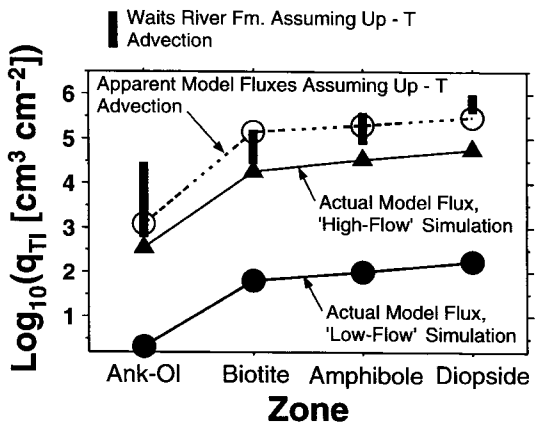

Fig. 12. Apparent and actual time-integrated fluid fluxes (q_{TI}) for metacarbonate mineral zones. Black bars, range in q_{TI} given by Ferry (1992, table 12) assuming up-T advection. ○, apparent q_{TI} calculated assuming up-T advection for typical 'low-flow' simulation (Fig. 3) and 'high-flow' simulation (Fig. 10; $\Delta X_{CO_2} = 7{\cdot}5 \times 10^{-4}$). Values computed using $\nabla T = 10^{-4}$°C/cm (Ferry, 1992, 1994) and the midpoint model T and maximum reaction progress attained for each mineral zone. Filled symbols, actual peak q_{TI} attained for the 'low-flow' and 'high-flow' simulations.

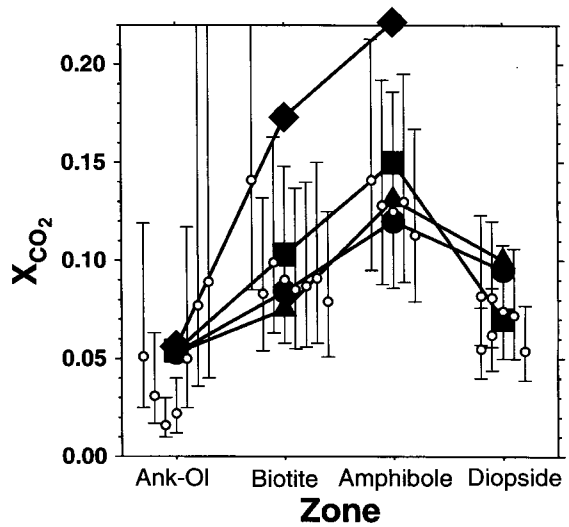

Fig. 13. Progression of X_{CO_2} as a function of metamorphic grade. ○, results for Waits River Formation of central–eastern Vermont (Ferry, 1992; samples 21-35C, 26-11B, 21-2F, 21- 23D of Ferry, 1994). Results recomputed for 7·8 kbar using the TWEEQU program of Berman (1991), the activity model of Holland & Blundy (1994) for plagioclase, and the activity models of Léger & Ferry (1993) for all other solids. Error bars correspond to a conservative ±15°C uncertainty in T. Peak model X_{CO_2} for typical 'low-flow' simulations involving limited advection and significant cross-layer diffusion shown as follows: (1) ● (metacarbonate layer of 5 m thickness; Fig. 3); (2) ■ (layer of 1 m thickness, metacarbonate/metapelite ratio = 0·25; Fig. 8a); (3) ◆ (layer of 1 m thickness, metacarbonate/metapelite ratio = 0·50; Fig. 8a). ▲, Peak X_{CO_2} for representative 'high-flow' simulation dominated by layer-parallel flow (see Fig. 10; $\Delta X_{CO_2} = 7{\cdot}5 \times 10^{-4}$).

before accurate flux estimates can be made (see Yardley, 1986; Bickle, 1992; Kohn & Valley, 1994).

Stable isotopic evidence suggests that fluids derived from or equilibrated with magmas probably augmented the regional dehydration flux in the deep crustal Diopside zone (e.g. Palin, 1992; Stern *et al.*, 1992; van Haren *et al.*, 1996). Interpretation of Diopside zone reaction progress in the Waits River Formation based on up-T advective input of magmatic fluids has been carried out (Ferry, 1992, 1994) but is problematic because local plutons are too small to provide the quantity of H_2O implied by the q_{TI} estimates (Ferry, 1992, p. 89). However, input of H_2O-rich magmatic fluids directly into metacarbonate layers may have produced much larger fluid concentration gradients than those arising solely from T gradients [denominator of equation (11)]. Consequently, Diopside zone q_{TI} estimates based on equation (11) may be overestimated, and the fluid mass balance problem may be largely an artifact of such overestimates.

Our work predicts that peak X_{CO_2} will typically increase from the Ankerite–Oligoclase to the Amphibole zones, but then drop in the Diopside zone (Figs 7, 8a and 10). X_{CO_2} values for many representative simulations and for field data from the Waits River Formation in central–eastern Vermont are indistinguishable (Fig. 13), demonstrating that our models can account for observed T-X_{CO_2} relations. However, the simulations indicate that diopside-producing reactions will not begin in high metacarbonate/metapelite ratio outcrops in which dehydration of local metapelitic rocks is the only H_2O source (Fig. 13). Diopside growth in these outcrops appears to require externally derived H_2O (Ferry, 1992, 1994), perhaps derived from crystallizing intrusions or dehydrating schists.

During prograde devolatilization, the X_{CO_2} of the surroundings will tend to rise and fall in sympathy with the X_{CO_2} of reacting metacarbonate layers (Fig. 5). Consequently, the peak X_{CO_2} reached in dehydrating metapelitic and metapsammitic layers intercalated with devolatilizing metacarbonates may tend to increase from the Ankerite–Oligoclase to Amphibole zones and then decrease in the Diopside zone. The magnitude of the changes will be greatest near lithologic contacts, and lessen as distance from contacts increases. Thus, increases of X_{CO_2} with grade recorded by metapelitic and metapsammitic rocks (Ferry, 1994) may not indicate pervasive, up-T flow throughout the entire region.

Implications for metasomatic zoning and reaction time scales

Spatial zonation of mineral assemblages within metacarbonate beds provides further tests of reaction progress scenarios. A key model prediction is that reaction progress

should be greatest where fluid composition gradients are steepest, such as adjacent to lithologic contacts and flow conduits. Furthermore, reaction fronts are predicted to be broader at low grades (Ankerite–Oligoclase, Biotite zones) than at higher grades, mostly because of the importance of solid solution in plagioclase at low grades and the general increase in reaction rates with T. These predictions are subject to considerable uncertainties stemming from uncertainties on the reaction rate constants, reactive surface areas, porosities, and solid solution systematics used in the modeling. None the less, the predictions are qualitatively consistent with the field relations discovered by Hewitt (1973) in the Wepawaug Schist. Mineral assemblage zonation adjacent to lithologic contacts and flow conduits in northern New England remains to be documented.

Fluid compositional gradients may be steep in alteration selvages directly adjacent to major flow conduits. The time needed for significant (~10 cm scale) penetration of selvages into metacarbonate rocks is predicted to be as short as 10^3–10^4 years (Fig. 9). These short time scales are consistent with oxygen isotopic data for metacarbonate and metapelitic rocks of the Wepawaug Schist (Palin, 1992; van Haren *et al.*, 1996) and metapelitic rocks of the Gassetts Schist, Vermont (Young & Rumble, 1993). For example, the vein surrounded by the Wep-8g selvage in the Wepawaug Schist contains quartz crystals having isotopically distinctive, relatively small $\delta^{18}O$ values of 13–14‰ (Tracy *et al.*, 1983; Palin, 1992). The vein-forming fluids may have been derived from or equilibrated with peraluminous syn-amphibolite facies intrusions (Palin, 1992; van Haren *et al.*, 1996). Transport-reaction theory modeling of oxygen isotope systematics for the Wep-8g selvage and several other Wepawaug metacarbonate rocks indicates that time scales of fluid–rock interaction were $<10^4$ years (Palin, 1992). Diffusional models of grain-scale oxygen isotope relations (van Haren *et al.*, 1996) suggest that the interaction of the isotopically light fluids with kyanite zone metapelite also took place in 10^3–10^4 years. If the flow was episodic rather than continuous, the total time of fluid–rock interaction could have been longer.

The modeling suggests that prograde metamorphism involves a large range in time scales of fluid–rock interaction. Slow reaction progress in metacarbonate rocks caused by progressive dehydration of surrounding metapelite from greenschist to amphibolite facies probably requires 10^6–10^7 my (Fig. 6)—time scales comparable to the duration of the Acadian orogeny. This slow metamorphic evolution may be punctuated by episodes of fracturing and intense fluid flow that form veins and selvages in as little as 10^3–10^4 years (Fig. 9). We speculate that short bursts of fluid activity may be related to fracturing and permeability increases associated with seismic moment release and earthquakes (e.g. Sibson *et al.*, 1975; Ague *et al.*, 1998), but much further work remains to establish or refute such a connection.

Our results indicate that study of fossil gradients in fluid composition between different rock types will be invaluable for determining mass transfer processes in New England. However, because such gradients can be extremely subtle and still drive major reaction progress (Figs 5 and 8b), careful field sampling strategies and petrological analysis will be required. Mapping of reaction front shapes will put much-needed constraints on the kinetics of metamorphic devolatilization and guide future laboratory experiments.

CONCLUSION

Models of Acadian reaction progress, T–X_{CO_2} relations, and fluid fluxes for metacarbonate layers in two parts of New England suggest an important role for exchange of CO_2 and H_2O between such layers and elevated X_{H_2O}/X_{CO_2} fluids derived from, for example, dehydrating metapelites or degassing magmas. Reaction progress is envisioned to be driven largely by gradients in fluid composition between different rock types (see Hewitt, 1973). Mass transfer may occur across lithologic contacts and involve substantial diffusion and/or occur by flow through metacarbonate layers. Our results do not require pervasive up-T flow through the metacarbonate layers themselves or horizontal fluid motion and are, therefore, consistent with physical models of deep crustal (>15–20 km) metamorphism that suggest that fluid flow is dominantly upwards and down-T (e.g. Walther & Orville, 1982; Connolly, 1997; Hanson, 1997). However, up-T flow is not precluded by our models. Our results support the conclusions of Hewitt (1973) and Ferry (1983, 1992, 1994) that progressive metamorphism of metacarbonate layers during Acadian orogenesis in New England involved progressively greater degrees of fluid–rock interaction.

ACKNOWLEDGEMENTS

We thank E. W. Bolton, P. D. Ihinger, A. C. Lasaga, A. Lüttge, J. M. Palin, and J. V. H. van Haren for discussions. The content and clarity of the paper were greatly improved by the critical and thoughtful reviews of J. M. Ferry, M. L. Gerdes, and J. V. Walther, and by the editorial comments of S. S. Sorensen. Financial support from National Science Foundation Grant EAR-9706638 and Department of Energy Grant DE-FG02-90ER14153 is gratefully acknowledged.

REFERENCES

Ague, J. J. (1994*a*). Mass transfer during Barrovian metamorphism of pelites, south–central Connecticut, I: Evidence for changes in composition and volume. *American Journal of Science* **294,** 989–1057.

Ague, J. J. (1994*b*). Mass transfer during Barrovian metamorphism of pelites, south–central Connecticut, II: Channelized fluid flow and the growth of staurolite and kyanite. *American Journal of Science* **294,** 1061–1134.

Ague, J. J. (1995). Deep crustal growth of quartz, kyanite, and garnet into large aperture, fluid-filled fractures, north-eastern Connecticut, USA. *Journal of Metamorphic Geology* **13,** 299–314.

Ague, J. J. (1997). Crustal mass transfer and index mineral growth in Barrow's garnet zone, Northeast Scotland. *Geology* **25,** 73–76.

Ague, J. J. (1998). Simple models of coupled fluid infiltration and redox reactions in the crust. *Contributions to Mineralogy and Petrology* **132,** 180–197.

Ague, J. J. & van Haren, J. L. M. (1996). Assessing metasomatic mass and volume changes using the bootstrap, with application to deep-crustal hydrothermal alteration of marble. *Economic Geology* **91,** 1169–1182.

Ague, J. J., Park, J. J. & Rye, D. M. (1998). Regional metamorphic dehydration and seismic hazard. *Geophysical Research Letters* **25,** 4221–4224.

Anderson, M. P. (1979). Using models to simulate the movement of contaminants through groundwater flow systems. *Critical Reviews in Environmental Control* **9,** 97–156.

Balashov, V. N. & Yardley, B. W. D. (1998). Modeling metamorphic fluid flow with reaction–compaction–permeability feedbacks. *American Journal of Science* **298,** 441–470.

Baumgartner, L. P. & Ferry, J. M. (1991). A model for coupled fluid-flow and mixed-volatile mineral reactions with applications to regional metamorphism. *Contributions to Mineralogy and Petrology* **106,** 273–285.

Bear, J. (1972). *Dynamics of Fluids in Porous Media.* New York: Elsevier, 764 pp.

Berman, R. G. (1988). Internally-consistent thermodynamic data for minerals in the system Na_2O–K_2O–CaO–MgO–FeO–Fe_2O_3–Al_2O_3–SiO_2–TiO_2–H_2O–CO_2. *Journal of Petrology* **29,** 445–522.

Berman, R. G. (1991). Thermobarometry using multi-equilibrium calculations: a new technique, with petrological applications. *Canadian Mineralogist* **29,** 833–855.

Bickle, M. J. (1992). Transport mechanisms by fluid-flow in metamorphic rocks: oxygen and strontium decoupling in the Trois Seigneurs Massif—a consequence of kinetic dispersion? *American Journal of Science* **292,** 289–316.

Bickle, M. J., Chapman, H. J., Ferry, J. M., Rumble, D., III & Fallick, A. E. (1997). Fluid flow and diffusion in the Waterville Limestone, south–central Maine: constraints from strontium, oxygen, and carbon isotope profiles. *Journal of Petrology* **38,** 1489–1512.

Bolton, E. W., Lasaga, A. C. & Rye, D. M. (1996). A model for the kinetic control of quartz dissolution and precipitation in porous media flow with spatially variable permeability: formulation and examples of thermal convection. *Journal of Geophysical Research* **101,** 22157–22187.

Boucher, D. F. & Alves, G. E. (1959). Dimensionless numbers for fluid mechanics, heat transfer, mass transfer, and chemical reaction. *Chemical Engineering Progress* **55,** 55–64.

Brimhall, G. H., Jr (1977). Early fracture-controlled disseminated mineralization at Butte, Montana. *Economic Geology* **72,** 37–59.

Brimhall, G. H., Jr (1979). Lithologic determination of mass transfer mechanisms of multiple-stage porphyry copper mineralization at Butte, Montana: vein formation by hypogene leaching and enrichment of potassium silicate protore. *Economic Geology* **74,** 556–589.

Carpenter, M. A. & Ferry, J. M. (1984). Constraints on the thermodynamic mixing properties of plagioclase. *Contributions to Mineralogy and Petrology* **87,** 138–148.

Centrella, J. & Wilson, J. R. (1984). Planar numerical cosmology. II. The difference equations and numerical tests. *Astrophysical Journal Supplement Series* **54,** 229–249.

Chamberlain, C. P. & Rumble, D. (1988). Thermal anomalies in a regional metamorphic terrane: an isotopic study of the role of fluids. *Journal of Petrology* **29,** 1215–1232.

Connolly, J. A. D. (1997). Devolatilization-generated fluid pressure and deformation-propagated fluid flow during prograde regional metamorphism. *Journal of Geophysical Research* **102,** 18149–18173.

David, C., Wong, T., Zhu, W. and Zhang, J. (1994). Laboratory measurement of compaction-induced permeability change in porous rock: implications for the generation and maintenance of pore pressure excess in the crust. *Pure and Applied Geophysics* **143,** 425–456.

Dullien, F. A. L. (1979). *Porous Media Fluid Transport and Pore Structure.* New York: Academic Press, 396 pp.

England, P. C. & Thompson, A. B. (1984). Pressure–temperature–time paths of regional metamorphism I. Heat transfer during the evolution of regions of thickened continental crust. *Journal of Petrology* **25,** 894–928.

Ferry, J. M. (1983). On the control of temperature, fluid composition, and reaction progress during metamorphism. *American Journal of Science* **283A,** 201–232.

Ferry, J. M. (1992). Regional metamorphism of the Waits River Formation, eastern Vermont; delineation of a new type of giant metamorphic hydrothermal system. *Journal of Petrology* **33,** 45–94.

Ferry, J. M. (1994). Overview of the petrologic record of fluid flow during regional metamorphism in northern New England. *American Journal of Science* **294,** 905–988.

Ferry, J. M. & Dipple, G. M. (1991). Fluid flow, mineral reactions, and metasomatism. *Geology* **19,** 211–214.

Fritts, C. E. (1965). Bedrock geologic map of the Ansonia quadrangle, Fairfield and New Haven Counties, Connecticut. *US Geological Survey Quadrangle Map GQ-426.*

Garven, G. & Freeze, R. A. (1984). Theoretical analysis of the role of groundwater flow in the genesis of stratabound ore deposits. 1. Mathematical and numerical model. *American Journal of Science* **284,** 1085–1124.

Haar, L., Gallagher, J. S. & Kell, G. S. (1984). *NBS/NRC Steam Tables. Thermodynamic and Transport Properties and Computer Programs for Vapor and Liquid States of Water in SI Units.* Washington, DC: Hemisphere.

Hanson, R. B. (1997). Hydrodynamics of regional metamorphism due to continental collision. *Economic Geology* **92,** 880–891.

Hawley, J. F., Smarr, L. L. & Wilson, J. R. (1984). A numerical study of nonspherical black hole accretion. II. Finite differencing and code calibration. *Astrophysical Supplement Series* **55,** 211–246.

Hewitt, D. A. (1973). The metamorphism of micaceous limestones from south–central Connecticut. *American Journal of Science* **273A,** 444–469.

Holland, T. & Blundy, J. (1994). Non-ideal interactions in calcic amphiboles and their bearing on amphibole–plagioclase thermometry. *Contributions to Mineralogy and Petrology* **116,** 433–447.

Holloway, J. R. (1987). Igneous fluids. In: Carmichael, I. S. E. & Eugster, H. P. (eds) *Thermodynamic Modeling of Geological Materials: Minerals, Fluids, and Melts. Mineralogical Society of America, Reviews in Mineralogy* **17,** 211–233.

Johnson, J. W., Oelkers, E. H. & Helgeson, H. C. (1992). SUPCRT92: a software package for calculating the standard molal thermodynamic properties of minerals, gases, aqueous species, and reactions from 1

to 5000 bars and 0° to 1000°C. *Computers and Geosciences* **18,** 899–947.

Kerrick, D. M. & Caldeira, K. (1998). Metamorphic CO_2 degassing from orogenic belts. *Chemical Geology* **145,** 213–232.

Kerrick, D. M. & Jacobs, G. K. (1981). A modified Redlich–Kwong equation for H_2O, CO_2, and H_2O–CO_2 mixtures at elevated temperatures and pressures. *American Journal of Science* **281,** 735–767.

Kohn, M. J. & Valley, J. W. (1994). Oxygen isotopic constraints on metamorphic fluid flow, Townshend Dam, Vermont, USA. *Geochimica et Cosmochimica Acta* **58,** 5551–5566.

Lanzirotti, A. & Hanson, G. N. (1996). Geochronology and geochemistry of multiple generations of monazite from the Wepawaug Schist, Connecticut, USA: implications for monazite stability in metamorphic rocks. *Contributions to Mineralogy and Petrology* **125,** 332–340.

Lasaga, A. C. (1986). Metamorphic reaction rate laws and development of isograds. *Mineralogical Magazine* **50,** 359–373.

Lasaga, A. C. & Rye, D. M. (1993). Fluid flow and chemical reaction kinetics in metamorphic systems. *American Journal of Science* **293,** 361–404.

Léger, A. & Ferry, J. M. (1993). Fluid infiltration and regional metamorphism of the Waits River Formation, northeast Vermont, USA. *Journal of Metamorphic Geology* **11,** 3–29.

Mäder, U. K. & Berman, R. G. (1991). A high pressure equation of state for carbon dioxide consistent with phase equilibrium and *P–V–T* data. *American Mineralogist* **76,** 1547–1559.

Meyer, C. (1965). An early potassic type of wall-rock alteration at Butte, Montana. *American Mineralogist* **50,** 1717–1722.

Morton, K. W. & Mayers, D. F. (1994). *Numerical Solution of Partial Differential Equations.* Cambridge: Cambridge University Press, 227 pp.

Nigrini, A. (1970). Diffusion in rock alteration systems: I. Prediction of limiting equivalent ionic conductances at elevated temperatures. *American Journal of Science* **269,** 65–91.

Palin, J. M. (1992). Stable isotope studies of regional metamorphism in the Wepawaug Schist, Connecticut. Ph.D. Thesis, Yale University.

Press, W. H., Teukolsky, S. A., Vetterling, W. T. & Flannery, B. P. (1992). *Numerical Recipes in FORTRAN,* 2nd edn. New York: Cambridge University Press, 963 pp.

Rye, D. M. & Rye, R. O. (1974). Homestake gold mine, South Dakota: I. Stable isotope studies. *Economic Geology* **69,** 293–317.

Saxena, S. K. & Fei, Y. (1987*a*). High pressure and high temperature fluid fugacities. *Geochimica et Cosmochimica Acta* **51,** 783–791.

Saxena, S. K. & Fei, Y. (1987*b*). Fluid at crustal temperatures and pressures. 1. Pure species. *Contributions to Mineralogy and Petrology* **95,** 370–375.

Selverstone, J. & Gutzler, D. S. (1993). Post-125 Ma carbon storage associated with continent–continent collision. *Geology* **21,** 885–888.

Sibson, R. H., Moore, J. M. & Rankin, A. H. (1975). Seismic pumping—a hydrothermal fluid transport mechanism. *Journal of the Geological Society, London* **131,** 653–659.

Spear, F. S. & Harrison, T. M. (1989). Geochronologic studies in central New England I: Evidence for pre-Acadian metamorphism in eastern Vermont. *Geology* **17,** 181–184.

Stern, L. A., Chamberlain, C. P., Barnett, D. E. & Ferry, J. M. (1992). Stable isotopic evidence for regional-scale fluid migration in a Barrovian metamorphic terrane, Vermont, U.S.A. *Contributions to Mineralogy and Petrology* **112,** 475–489.

Tracy, R. J., Rye, D. M., Hewitt, D. A. & Schiffries, C. M. (1983). Petrologic and stable-isotopic studies of fluid–rock interactions, south-central Connecticut: I. The role of infiltration in producing reaction assemblages in impure marbles. *American Journal of Science* **283A,** 589–616.

van Haren, J. L. M., Ague, J. J. & Rye, D. M. (1996). Oxygen isotope record of fluid infiltration and mass transfer during regional metamorphism of pelitic schist, south-central Connecticut, USA. *Geochimica et Cosmochimica Acta* **60,** 3487–3504.

Vidale, R. J. & Hewitt, D. A. (1973). 'Mobile' components in the formation of calc-silicate bands. *American Mineralogist* **58,** 991–997.

Walder, J. & Nur, A. (1984). Porosity reduction and crustal pore pressure development. *Journal of Geophysical Research* **89,** 11539–11548.

Walther, J. V. (1996). Fluid production and isograd reactions at contacts of carbonate-rich and carbonate-poor layers during progressive metamorphism. *Journal of Metamorphic Geology* **14,** 351–360.

Walther, J. V. & Orville, P. M. (1982). Volatile production and transport in regional metamorphism. *Contributions to Mineralogy and Petrology* **79,** 252–257.

Wong, T., Ko, S. & Olgaard, D. L. (1997). Generation and maintenance of pore pressure excess in a dehydrating system 2. Theoretical analysis. *Journal of Geophysical Research* **102,** 841–852.

Yardley, B. W. D. (1986). Fluid migration and veining in the Connemara schists, Ireland. In: Walther, J. V. & Wood, B. J. (eds) *Fluid–Rock Interactions during Metamorphism.* New York: Springer-Verlag, pp. 109–131.

Young, E. D. & Rumble, D., III (1993). The origin of correlated variations in *in-situ* $^{18}O/^{16}O$ and elemental concentrations in metamorphic garnet from southeastern Vermont, USA. *Geochimica et Cosmochimica Acta* **57,** 2585–2597.

APPENDIX A

Numerical solution

Equations (1) and (6) were solved using standard explicit finite difference techniques. The Forward Time Centered Space method was used for diffusive terms; first-order upwind differencing was used for advective terms in most simulations (see Press *et al.*, 1992; Morton & Mayers, 1994). The upwind scheme proved adequate for the low Peclet number simulations, but the layer-parallel advection simulations benefited from higher-accuracy treatment of the advective term of equation (1) using Barton's method (see Centrella & Wilson, 1984; Hawley *et al.*, 1984; Ague, 1998). The solutions account for spatially and temporally varying fluid composition, reaction rates, pore velocities, φ, and κ. Treatment of coupled transport and chemical reaction follows Ague (1998).

Grid spacings and time steps were varied from 1 to 100 cm and $7{\cdot}0 \times 10^{-5}$ to $1{\cdot}0 \times 10^{1}$ years, respectively, depending upon the degree of spatial and temporal resolution desired. Time-integrated mass balances for H_2O and CO_2 across contacts between model metacarbonate and metapelite layers for a representative simulation (Fig. 3) agree within 0·2% of the exact values based on metacarbonate mode and dehydration rate of metapelite. Additional algorithm verification was carried out following Ague (1998); numerical dissipation and dispersion were insignificant.

Thermodynamic and kinetic data

The free energy changes needed for equations (3) and (4) were computed using standard state thermodynamic data for solids and gases taken from Berman (1988, 1991) and Johnson *et al.* (1992), respectively. The pressure–volume–temperature relations of the pure gas end-members were computed using a modified Redlich–Kwong equation of state below 4 kbar (see Holloway, 1987) and the methods of Saxena & Fei (1987*a*, 1987*b*) at higher pressures (see Ague, 1998). The advantage of the Saxena & Fei expressions is that they are relatively simple and can therefore be rapidly computed. H_2O–CO_2 mixtures were treated following Kerrick & Jacobs (1981). These thermodynamic data and fugacity relations yield results nearly identical to those of the TWEEQU program of Berman (1991), which uses by default the Kerrick & Jacobs (1981) model for H_2O–CO_2 mixtures and the equations of state of Haar *et al.* (1984) for H_2O and Mäder & Berman (1991) for CO_2. Organic matter is present in many metacarbonate units (see Ferry, 1992, 1994; Ague & van Haren, 1996), but Ferry (1992) has argued that reduced species (e.g. H_2, CO, CH_4, H_2S) typically make up only a small portion of the fluid.

We use the nonlinear kinetic parameters of Lasaga & Rye (1993) to model rates of fluid–rock reaction in the metacarbonate layers: $k_j^\circ = 1{\cdot}38 \times 10^{-14}$ mol/cm^2 per year (J/mol)$^{-n_j}$; $n_j = 2{\cdot}68$; $Ea = 8{\cdot}37 \times 10^4$ J/mol; and $T^\circ = 873{\cdot}15$ K (600°C). The rate-limiting surface area, $\bar{A}_{ij}$, was set to 1 cm^2/cm^3 corresponding to, for example, 1 vol. % of grains of 300 μm radius; Ague (1998) discussed models in which $\bar{A}_{ij}$ varies with time. These rate parameters yield a relatively close approach to local fluid–rock equilibrium in that large reaction oversteps do not occur. Kinetic effects we did not consider, such as nucleation-induced overstepping, may be significant in some natural systems (Lasaga, 1986; Ague *et al.*, 1998).

Activity–composition relations for minerals

We assumed that most solids are pure end-member phases; Fe–Mg solid solution (see Ferry, 1992) has a relatively small effect on the positions of the univariant curves we consider. However, this assumption is insufficient for plagioclase (Pl), because X_{An} increases with increasing grade from $\leq 0{\cdot}1$ in the lower–middle greenschist facies to ~0·2–0·9 at higher grades (see Hewitt, 1973; Ferry, 1992, 1994). We assumed that Pl was homogeneous during each step of reaction progress and calculated activity–composition relations using the model of Holland & Blundy (1994). Compositional zoning (e.g. Hewitt, 1973; Ferry, 1992) and metasomatism involving feldspar components (e.g. Tracy *et al.*, 1983; Ague & van Haren, 1996) are important phenomena in many natural systems, but are beyond the scope of this paper.

APPENDIX B

Pressure and temperature for Wep-8g simulation

Sample Wep-8g of Hewitt (1973) and Tracy *et al.* (1983) lies within the Kyanite zone of Ague (1994*a*). Peak pressures were probably 7–9 kbar (Ague, 1994*b*); we use 8 kbar for the initial P_f in the center of the layer. A T of ~600°C is reasonable based on chemical and isotopic thermometry for the kyanite zone (Ague, 1994*b*; van Haren *et al.*, 1996). The T of reaction was probably slightly below the intersection of the equilibrium curve for reaction (6) with those for reactions (4), (5), and (7) (Tracy *et al.*, 1983). For the thermodynamic data and activity models used here at 8 kbar, this topology suggests T of ~590°C (863·15 K), which we used in the calculations.